A Distributed Lag-Autoregressive Model of Geostationary Relativistic Electron Fluxes: Comparing the Influences of Waves, Seed and Source Electrons, and Solar Wind Inputs

Laura Simms[1], Mark Engebretson[1], Mark Clilverd[2], Craig Rodger[3], Marc Lessard[4], Jesper Gjerloev[5], and Geoffrey Reeves[6]

[1] Department of Physics, Augsburg University, Minneapolis, MN, USA

[2] British Antarctic Survey (NERC), Cambridge, UK

[3] Department of Physics, University of Otago, Dunedin, New Zealand

[4] University of New Hampshire, Durham, New Hampshire, USA

[5] Johns Hopkins University, Laurel, MD, USA

[6] Los Alamos National Laboratory, Los Alamos, New Mexico, USA

Corresponding author: Laura E. Simms (simmsl@augsburg.edu)

Key Points:

1. ULF Pc5 and chorus waves contribute equally to relativistic electron flux enhancement. Loss due to EMIC waves is less influential
2. Distributed lag models show influences are limited to 0-2 days
3. Injection of high energy electrons by substorms is at least as important as acceleration by wave action at some energies

Abstract

Relativistic electron flux at geosynchronous orbit depends on enhancement and loss processes driven by ULF Pc5, chorus, and EMIC waves, seed electron flux, magnetosphere compression, the "Dst effect", and substorms, while solar wind inputs such as velocity, number density, and IMF Bz drive these factors and thus correlate with flux. Distributed lag regression models show the time delay of highest influence of these factors on $\log_{10}$ high energy electron flux (0.7 – 7.8 MeV, LANL satellites). Multiple regression with an autoregressive term (flux persistence) allows direct comparison of the magnitude of each effect while controlling other correlated parameters. Flux enhancements due to ULF Pc5 and chorus waves are of equal importance. The direct effect of substorms on high energy electron flux is strong, possibly due to injection of high energy electrons by the substorms themselves. Loss due to EMIC waves is less influential. Southward Bz shows only moderate influence when correlated processes are accounted for. Adding covariate compression effects (pressure and IMF magnitude) allows wave-driven enhancements to be more clearly seen. Seed electrons (270 keV) are most influential at lower relativistic energies, showing that such a population must be available for acceleration. However, they are not accelerated directly to the highest energies. Source electrons (31.7 keV) show no direct influence when other factors are controlled. Their action appears to be indirect via the chorus waves they generate. Determination of specific effects of each parameter when studied in combination will be more helpful in furthering modelling work than studying them individually.

1. Introduction

The level of relativistic electron flux in the radiation belts at geosynchronous orbit is the result of a balance between enhancement and loss processes (Reeves et al., 2003). Increases in flux may be due to energization of lower energy particles already present through wave-particle interactions. Decreases may also result from wave activity driving precipitation into the atmosphere or transport by radial diffusion to higher L-shells and subsequent escape through the magnetopause. In this study, through statistical techniques, we investigate the relative importance and combined influence of ULF Pc5 (ultralow frequency), lower band VLF (very low frequency) chorus, and EMIC (electromagnetic ion cyclotron) waves as well as the time scales of their action on relativistic electron flux at geosynchronous orbit. The processes described below are summarized in Figure 1.

1.1 ULF Pc5 waves

ULF Pc5 waves (150-600s; 2-7 mHz) are produced at the magnetopause as a result of velocity shear or solar wind pressure fluctuations (Ukhorskiy et al., 2006; Takahashi & Ukhorskiy, 2007), with less contribution from internal sources such as instability of the magnetospheric plasma (Liu et al., 2009; Kessel, 2008). They can migrate inwards to lower L shells and may accelerate electrons to relativistic energies via several proposed mechanisms. For example, drift resonance interactions between seed electrons (in the hundreds of keV range) and toroidal ULF Pc5 waves may transport and energize the electrons by inward radial diffusion (Falthammar, 1965; Elkington et al., 1999; Hudson et al., 2000; Nakamura et al., 2002; Ukhorskiy et al., 2005) , although it has been found that the available ULF Pc5 wave power necessary for this process drops off rapidly at lower L-shells (Mathie & Mann, 2001) and may decay further while the radiation belts are reforming following storms (Horne et al., 2005b). In addition, the peak of electron phase space density occurs near L-shell 4-5, indicating local acceleration in that location rather than transport from higher L-shells (Chen et al., 2006, Iles et al., 2006). Besides this, modeling has shown that the observed rates of electron acceleration are faster than would be predicted by radial diffusion (Brautigam & Albert, 2000; Shprits et al., 2006). This has led to doubts that radial diffusion processes are responsible for much of the flux increases in >1MeV electrons at geosynchronous orbit (O'Brien et al., 2003; Horne et al., 2005b). Compressional ULF Pc5 waves may energize electrons through transit time damping (Summers & Ma, 2000b; Li et al., 2005; Clausen et al., 2011), and poloidal ULF Pc5 waves may also play a role via magnetic pumping (Liu et al., 1999; Elkington et al., 2003; Ren et al., 2015; Shah et al., 2016). There may also be nonresonant interactions with ULF Pc5 waves that accelerate electrons stochastically over shorter time scales, which could provide more rapid acceleration of electrons by ULF Pc5 waves (Shah et al*.,* 2015*;* Ukhorskiy et al*.,* 2009; Degeling et al., 2013).

Whichever ULF Pc5-driven processes are at work, however, observations do show that ULF Pc5 waves are strongly correlated with flux increases at geosynchronous orbit (Rostoker et al., 1998; Mathie & Mann, 2000; O'Brien et al., 2003; Mann et al., 2004; Degtyarev et al., 2009; Borovsky & Denton, 2014; Su et al., 2015; Simms et al., 2016; Lam, 2017). This is true even when other correlated predictors (ground-observed VLF waves, substorms, and solar wind parameters) are controlled for in a multiple regression analysis, showing that the ULF Pc5 effect is not simply a statistical artifact of Pc5 waves increasing concurrently with other physical parameters that are responsible for electron acceleration (Simms et al., 2014; 2016). In fact, in Simms et al. (2016) the correlation with ULF Pc5 waves was quite a bit stronger than that with VLF waves, suggesting that ULF Pc5 waves are the dominant wave driving electron acceleration. However, the ground-based VLF wave power used in these previous studies (from Halley, Antarctica) is known to be attenuated by trans-ionospheric propagation, particularly during summer months (Smith et al., 2010; Simms et al., 2015). Thus, it may not be a good proxy for space-based VLF chorus activity, and this may have given more apparent weight to the ULF Pc5 influence.

It should be mentioned that ULF Pc5 waves are also predicted to result in relativistic electron loss at geosynchronous orbit through outward radial diffusion during shock events (Degeling et al., 2008; Loto'aniu et al., 2010; Shprits et al., 2006; Ukhorskiy et al., 2009; 2015; Zong et al., 2012; Hudson et al., 2014; Brautigam & Albert, 2000).

1.2 VLF chorus waves

Cyclotron resonance of electrons with VLF chorus waves is another possible acceleration process (Summers et al., 1998; Meredith et al*.,* 2002; Li et al., 2005; Bortnik & Thorne, 2007; Summers et al., 2007; Thorne et al., 2010; Xiao et al., 2015). VLF Chorus is thought to originate from unstable distributions of electrons (several - 100 keV) injected from the plasmasheet during substorm activity (Meredith et al., 2001; 2003a; Tsurutani & Smith, 1974; Li et al., 2009; Su et al., 2014; Rodger et al., 2016), which follows increased solar wind speeds (Lyons et al., 2005). As these VLF chorus waves can resonate with electrons of many different energies, they could locally accelerate seed population electrons up to relativistic energies, although this appears to be more likely under conditions of southward Bz (Miyoshi et al., 2013). It has been postulated that these local acceleration processes (by both VLF chorus and ULF Pc5 waves) may be more important than radial diffusion (Thorne, 2010).

Lower band VLF chorus waves (0.1-0.5 of the electron cyclotron frequency (fce)) are thought to interact more effectively with energetic electrons than those in the upper band (Horne & Thorne, 1998; Meredith et al., 2002). In case studies using either ground or satellite data, higher intensity of lower band VLF chorus waves has been observed during periods of increasing relativistic electron flux (Meredith et al., 2002, 2003a; Miyoshi et al., 2003; 2007; O'Brien et al., 2003; Spasojevic & Inan, 2005; Horne et al., 2005a; Iles et al., 2006; Thorne et al., 2013; Turner et al., 2013; 2014). The intensification of VLF waves during the reforming of the radiation belts, when ULF Pc5 waves are simultaneously at their most monochromatic, has led to the hypothesis that VLF waves must be the primary driver of electron acceleration (Baker et al, 2004; Horne et al., 2005b; Bortnik & Thorne, 2007). Superposed epoch analyses also show higher levels of VLF chorus/whistler waves occurring with increased flux of energetic electrons (Smith et al., 2004 (Halley ground data); MacDonald et al., 2008 (proxy based on hot plasmasheet electron population); Li et al., 2014a, (proxy based on the ratio of the precipitated and trapped electron fluxes (30–100 keV))), but in a correlation analysis >2MeV electron flux was found to be less associated with VLF ground data than ULF Pc5 waves were (Simms et al., 2014; 2016). This lower correlation of chorus in the last studies may be an indication that chorus waves not only accelerate electrons but also cause their precipitation into the ionosphere through pitch-angle scattering into the loss cone (Lorentzen et al., 2001; Bortnik & Thorne, 2007; Millan and Thorne 2007; Bortnik et al., 2006; Lam et al., 2010; Hikishima et al., 2010; Orlova and Shprits, 2010; Hendry et al., 2012), particularly at higher latitudes (Horne & Thorne, 2003). Oblique angled chorus waves could also reduce the seed electron population (Mourenas et al., 2016). Thus, the sum effect of chorus on flux levels, increases from acceleration and decreases from precipitation and reducing the seed population, could be modest overall.

However, as mentioned in the previous section, the use of VLF ground data is problematic due to attenuation. Proxy measures may also not be ideal. A proxy could introduce spurious correlations into the analysis if the predicted variable (high energy electron flux) is also correlated with the basis of the proxy. For example, the use of microburst precipitation data to infer VLF chorus activity confounds the direct measure of electron loss (precipitation) with the process that supposedly drives the loss (the chorus activity) (Lorentzen et al., 2001; O'Brien et al., 2003; 2004). Thus there is no independent means of verifying that VLF chorus correlates with the precipitation that is being measured.

A better approach to answering the question of whether ULF Pc5 or VLF chorus waves are the more important influence on flux would use satellite VLF data instead of proxies or ground data. Although case studies show VLF chorus contributing to both acceleration and loss individually (Turner et al., 2014), statistical correlational studies of the overall effect of chorus on flux using satellite data are scarce. We address this issue by using VLF chorus wave observations from the DEMETER satellite (Berthelier et al., 2006) instead of ground VLF data or the proxy microburst data.

1.3 EMIC Waves

Electromagnetic ion cyclotron (EMIC) Pc1 waves may cause precipitation of radiation belt electrons into the atmosphere through pitch angle scattering (Albert, 2003; Summers & Thorne, 2003; Usanova et al., 2014; Clilverd et al., 2007; 2015; Engebretson et al., 2015; Rodger et al., 2015). EMIC waves may be driven by a ring current pitch angle anisotropy due to protons injected during storms and substorms (Jordanova et al. 2008). They are more likely to occur during storms or periods of high solar wind pressure (Erlandson & Ukhorskiy, 2001; Halford et al., 2016; Usanova et al., 2012; Tetrick et al., 2017), being somewhat more likely in the main phase than recovery (Halford et al., 2010). Many are observed in quiet times as well (Saikin et al., 2016; Tetrick et al., 2017). Storms with high EMIC activity (as measured by a plasma proxy based on measurements from the LANL Magnetospheric Plasma Analyzer)) show higher electron losses (Blum et al., 2009), and EMIC wave activity is often seen when precipitation is occurring (Miyoshi et al., 2008; Rodger et al., 2008; Li et al., 2014b; Turner et al., 2014; Blum et al., 2015; Gao et al., 2015). EMIC waves may occur in both main phase and recovery (Fraser et al., 2010), but narrowband Pc1 waves are less likely to be seen by ground magnetometers during the main phase. In theory, EMIC waves will only precipitate electrons below 1–2MeV in areas with high plasma density (Jordanova et al., 2008). Therefore, they would presumably have more influence in reducing the measured flux of ultrarelativistic electrons (> 2MeV). In agreement with this, a strong energy dependence in electron depletion at L shells > 5 has been found (Bortnik et al., 2006), and the introduction of an EMIC parameter in the VERB model improves the model of these higher energy electrons (Drozdov et al., 2017). However, Ukhorskiy et al. (2010) have calculated that EMIC waves should be capable of scattering electrons with energies down to 400 keV, with observations showing that EMIC-driven precipitation is quite common below 1 MeV (Hendry et al., 2017). Additionally, broadband activity seen during the main phase of geomagnetic storms may also precipitate electrons (Engebretson et al., 2008).

1.4 Other causes of electron dropouts

There are other factors that could lead to temporary electron reductions or dropouts at geosynchronous orbit. The "Dst effect" refers to the decrease in geosynchronous flux seen in the main phase of storms when the ring current increases and the magnetic field strength is reduced (Li et al., 1997; Kim & Chan, 1997). As particles move outward due to the weaker magnetic field, their energy decreases adiabatically (Onsager et al., 2002). A second adiabatic process is the localized stretching of the magnetic field associated with substorms and increased solar wind pressure (Li et al., 1997). This stretching may move the trapping boundary inward which results in dropouts of particle fluxes observed by satellites situated in geosynchronous orbit (Onsager et al., 2002). Compression of the magnetosphere due to solar wind pressure can be intense enough that geosynchronous satellites are temporarily left outside the magnetosheath and therefore cannot "see" the radiation belt electrons (Dmitriev et al., 2014).

In addition, compression of the magnetosphere may allow trapped particles to cross the magnetopause and be permanently lost through magnetopause shadowing (Onsager et al., 2002; Yu et al., 2013; Herrera et al., 2016; Xiang et al., 2017). Although the adiabatic processes would allow flux to return to its pre-storm level when conditions relax back to less disturbed levels, magnetopause shadowing results in permanent loss of these particles. Simulations and satellite observations suggest that depletion due to movement of the magnetopause may be considerable and can be induced by either pressure spikes or southward Bz (Yu et al., 2013; Bortnik et al., 2006; Turner et al., 2013; Morley et al., 2010; Hudson et al., 2014; Turner et al., 2014; Gao et al., 2015). However, fluxes may also be enhanced when increased pressure and southward Bz occur simultaneously (Ni et al., 2016) or when southward Bz is combined with higher solar wind number density (Boynton et al., 2016). Magnetic shock events (increased IMF magnitude: |B|) can produce electric fields which accelerate electrons (Foster et al., 2015), and compression itself may lead to an electric field impulse which causes inward electron transport (Halford et al., 2015). Thus, while either pressure or the IMF could represent the degree to which magnetopause shadowing is occurring, these variables may also result in enhancement of flux.

1.5 Upstream drivers of wave activity

Ultimately, the energy that drives the waves investigated in this study comes from the solar wind and interplanetary magnetic field (IMF). ULF Pc5 waves are correlated with a variety of these external factors (e.g., Simms et al., 2010; 2016; Thorne, 2010; Claudepierre et al., 2008; Ukhorskiy et al., 2006; Degeling 2014; Mann et al., 2004; Paulikas and Blake, 1979) and are thought to be responding to geomagnetic activity driven by solar input (Walker, 1981; Cahill et al., 1990; Kepko & Spence, 2003; Tan et al., 2011). VLF chorus waves may be excited by cyclotron resonance with anisotropic plasmasheet electrons (several keV- 100 keV) injected during substorms (Anderson & Maeda, 1977; Hwang et al., 2007; Tsurutani & Smith, 1977; Li et al., 2013; Meredith et al., 2001; 2003a; Turner et al., 2015; Kissinger et al., 2014; Rodger et al., 2016) when the IMF is pointing southward (Miyoshi et al., 2013). Substorms and subsequent particle injections are themselves a result of increased solar wind driving (McPherron et al., 2009; Lyons et al., 2005). EMIC waves are also correlated with increased geomagnetic activity driven by solar wind conditions (Saikin et al., 2016; Anderson & Hamilton, 1993; Halford et al., 2010; Erlandson & Ukhorskiy, 2001; Usanova et al., 2012). These external influences are themselves highly correlated with each other (e.g., Borovsky, 2018). For this reason, various coupling factors have been proposed to model the transfer of energy between the solar wind and the magnetosphere (Newell et al., 2006). We briefly explore two simpler ones in this paper: -vBs and Ey, however, the inclusion of these factors individually (V or Bz) in a single analysis (e.g., multiple regression) may preclude the addition of these coupling factors.

1.6 Substorm influences

Substorms not only provide the so-called "source" electrons (several keV-100keV) whose anisotropies drive VLF chorus wave intensifications, they also inject the seed electrons (several hundreds of keV) that are accelerated to relativistic energies (Miyoshi et al., 2013; Jaynes et al., 2015; Turner et al., 2014; 2015; Tang et al., 2017). Without this injection, there will be no electrons to accelerate to high energies. Thus, substorm activity, and injection, is an essential element in increased high energy electron fluxes and no large flux enhancements are seen when substorm and lower-band chorus activity are low (Meredith et al., 2003a).

1.7 Analysis approach

This balance between processes that accelerate electrons, those that provide the seed electrons, and those that lead to loss or transport of high energy electrons should be considered simultaneously when building models of high-energy electron flux levels. Simple correlations do not give an accurate description of the effect of each on flux because this type of analysis does not account for correlation between predictors (Simms et al., 2014). Nor does correlation analysis give the relationship between variables, as it only provides information on the amount of scatter around the underlying relationship. Linear regression analysis, on the other hand, also gives the slope of the line describing the relationship between dependent and independent variables, as well as information on how well that line fits the data. An extension of linear regression is multiple regression, in which more than one predictor variable can be used to predict the outcome variable. This is a useful technique to apply when there are several possible predictors. The multiple regression analysis can provide information on the relative influence of each parameter on the outcome, as well as correct for the possible overlap in correlation that each predictor has with the dependent variable. Thus, multiple regression gives us the independent contribution from each predictor relative to other predictors, corrected for its possible association with other parameters (Neter et al., 1985).

Neural network analysis may be used to produce models similar to those obtained by regression (O'Brien & McPherron, 2003), however regression is better able to assess the relative influence of the explanatory variables (reported via the regression coefficients) on the modelled response variable. In addition, regression is better suited to prediction of quantitative response variables (e.g., flux) while neural networks model probabilities of categorical responses. Regression analysis is also similar to the multi-correlation method used by Borovsky (2017) which uses linear combinations of variables. However, the robustness of regression analysis and its ability to produce models that represent the data well and without bias has been more thoroughly explored as a standard technique of statistical analysis over many years. The multi-correlation of linear combinations with the final choice made by an "evolutionary" method is perhaps more properly classified as a subset of regression selection techniques (e.g., backward elimination, stepwise regression, etc.). However, automatic selection techniques (neural network analysis may also be classified as such) do have drawbacks in that the "best" selected model may have little relationship to physical processes (Derksen & Keselman, 1992; Harrell, 2015). For this reason, we build our models "by hand", considering first those physical processes that we believe have direct influences on electron levels ("internal" effects), separately considering the drivers of these internal processes ("external" effects), and then comparing the influences of both internal and external effects in the final model.

Previous work using cross correlations has shown that ULF Pc5 waves are most effective at predicting relativistic electron flux 2-3 days later (Mann et al., 2004; Kozyreva et al., 2007; Lam, 2017; Regi et al., 2015). Solar wind velocity has its highest correlation with flux at a two day lag (Kozyreva et al., 2007; Boynton et al., 2013; Zhao et al., 2017), and substorms show their most influence on flux at a 1-3 day lag (Forsyth et al., 2016). However, as the level of these parameters in each time period is often highly correlated with their level in nearby time periods, a comparison of simple correlations at each lag may hide important patterns. High correlations between observations at successive time steps could give the impression that a predictor acts over long periods of time, however it may only be influential during one particular time step. A distributed lag regression model extends the multiple regression model to the case where many lags of the predictor variable are entered simultaneously (Almon, 1965). With this approach, we can determine if all lags are important in predicting the dependent variable, or just a few.

However, one complication with using statistical analyses like regression on time series data is that correlation between time steps of the dependent variable can inflate significance tests. Each time step's measurement is not an independent observation. As electron flux changes little from day to day, we must correct for this problem by introducing previous day's flux as an autoregressive (AR) term (Simms et al., 2016). Electron persistence has also been tested and compared to more complicated models developed with a neural network procedure (O'Brien & McPherron, 2003) and incorporated into forecast models using solar wind parameters as well as waves to predict flux (Ukhorskiy et al., 2004; Kellerman et al., 2013; Sakaguchi et al., 2015; Borovsky, 2017).

The regression equations we test have both distributed lag terms (the value of the predictor variable over several time steps) as well as an autoregressive term (the value of the electron flux on the previous time step). For a single predictor (Pred), with flux measured at time t and all lags up to s included, the model is a linear equation:

$$Log\ Flux_t = b_0 + b_{AR} \times Log\ Flux_{t-1} + \sum_{i=0}^{s} b_i \times Pred_{t-s} \tag{1}$$

where each $\underline{b}$ is a regression coefficient: the b_0 being a constant term, the $\underline{b}_{AR}$ the coefficient associated with the autoregression of flux on itself one time step earlier and each $\underline{b}_i$ the coefficient associated with each time step of the predictor. Adding to the complexity, each of the processes acting on flux is associated with its own drivers, some of which may account for a portion of the flux response independently as well.

In our analyses, we first perform distributed lag, autoregressive models using single variables to predict $\log_{10}$ relativistic electron flux. From this, we determine at which lags the predictors act most strongly. We then analyze three wave types (ULF Pc5, VLF lower band chorus, and EMIC waves) at several lags in one regression model to compare their relative influences. Following this, we add "upstream" parameters that are thought to drive wave activity, several of which may be proxies for effects such as magnetopause shadowing.

2. Data and Methods

For the years 2005-2009, we use daily averaged log electron fluxes from the Los Alamos National Laboratory (LANL) satellites in geosynchronous orbit (Reeves et al., 2011). We use four energy channels of relativistic electrons measured by the Energetic Spectrometer for Particles (ESP) instrument (0.7-1.8, 1.8-3.5, 3.5-6.0, and 6.0-7.8 MeV; $\log_{10}$(electrons/(cm^2/s/sr/keV)) and two lower energy channels measured by the Synchronous Orbit Particle Analyzer (SOPA) instrument (source electron flux at 31.7 keV and seed electron flux at 270 keV in the same units as above). Daily averaged ULF Pc5 wave power was obtained from a ground-based ULF Pc5 index covering local times 0500 – 1500 in the Pc5 range (2-7 mHz) obtained from magnetometers stationed at 60-70° N CGM (Corrected GeoMagnetic) latitude (Kozyreva et al., 2007). This index includes both ULF Pc5 waves and turbulence in the ULF Pc5 range (Romanova et al., 2007). VLF lower band chorus ($\log_{10}$(μV^2/m^2/Hz)) daily-averaged intensity (0.1 - 0.5 fce, the electron cyclotron frequency) was obtained from the ICE (Instrument Champ Electrique) on the Demeter satellite (Berthelier et al., 2006). As this was a low-Earth orbit satellite focused on low latitude regions, most observations occurred in L shells 1-4. We use L = 4 (4.0-4.99), the highest L shell in which there is good data coverage, averaged over the dayside passes of the satellite (LT 10:30). We use dayside chorus because it is found over a broader range of latitudes than nightside chorus and is not as influenced by geomagnetic activity (Tsurutani & Smith, 1977; Li et al., 2009, Thorne et al., 2010). All of these datasets represent only a sample of overall global activity as satellites can only sample one small area of the magnetosphere at a time.

In addition, we obtained IMF Bz component, IMF magnetic field magnitude |B|, Dst, and solar wind velocity (V), number density (N), -VBz (Ey – electric field), and pressure from the Omniweb database. We use daily averages of all but Bz for which we use the fraction of hours per day with southward Bz. We also calculated -VBs by multiplying the hourly average of V and -Bz, setting negative (northward Bz) values to 0, and averaging over each day.

EMIC wave power data was obtained from the induction coil magnetometer located at the Halley, Antarctica BAS ground station at L shell 4.6. We use the number of hours per day at which there was high EMIC activity (> 10^{-3} nT^2 Hz) in the <1 Hz band. Only narrowband activity was included. The use of only one ground station may mean that we underestimate EMIC wave occurrence and its effectiveness in our models (Keika et al., 2013; Saikin et al., 2015).

We use the number of substorms per day from the SuperMAG substorm list (Gjerloev, 2012).

Analyses are performed for each of the four relativistic electron flux channels separately, using daily averages of the predictors. We use a variety of techniques to explore the relationship between predictors and relativistic electron flux. Distributed lag models, which enter all lags of a predictor into a multiple regression analysis, compare effects of each lag while other lags are controlled for. Each lagged variable is the predictor measured in the days preceding the flux measurement. We choose the most statistically significant lags from 0 to 5 days to use in multiple regression models including more than one predictor. We consider two submodels. The first is an internal effects model including ULF Pc5, VLF chorus, and EMIC waves together with seed electrons and Dst. We include lag 0 solar wind pressure and |B| as covariates to account for magnetopause shadowing and possibly for the compression of the radiation belts below the geosynchronous altitude of the LANL satellites. "Lag 0" measures predictors on the same day as the high energy electron flux. The second submodel is an external effects model including Bz, V, substorms, and source electrons, as well as three lags (0-2 days) of pressure and |B|, all of which are thought to drive the wave activity or seed electron fluxes. Finally, we perform several regression models including all variables (except N) using a) pressure, |B|, and Dst at lag 0 (representing compression and the "Dst effect"), and other variables at lag 1 day, and b) using the strongest lag of each variable at each energy level from the submodels. We report the standardized regression coefficients in the figures to compare magnitude of effects. The unstandardized coefficients are dependent on measurement scales of the predictors and therefore cannot be compared directly. The unstandardized coefficients, however, could be used to predict flux from a different dataset (Simms et al., 2014; 2016). We report these for use in future data-driven modelling efforts (Table 1). Statistically significant regression coefficients (p-value < .05) are generally represented as dark bars in the figures (the exception being Figure 2). Statistically significant effects at this p-value (< 0.05) mean that we have confidence that there is an actual association between the variables. Non-significant results (>0.05) mean we do not have evidence for correlation between parameters. The p-value gives the probability that the null hypothesis is true (i.e., no association) given the distribution of the data. Thus, a low p-value gives us reason to reject the null hypothesis and accept that there is an association between variables (Neter et al., 1985). The setting of 0.05 as the arbitrary level for statistical significance is well established (e.g., Cowles and Davis, 1982 for a historical perspective).

The addition of several correlated predictors to a regression model can result in high multicollinearity among the variables which increases variance of the regression coefficients. This increased variance may be problematic as it makes the coefficients unstable and therefore harder to interpret. For this reason, we check the variance inflation factor (VIF) statistic for each regression. A VIF=1 means the predictor variables are not at all correlated, while VIF>10 suggests that the issues may be severe enough to require correction (Neter et al., 1985). For all parameters in all models presented, VIF are less than 10 except for the lag 1 of solar wind velocity (V) in the external-effects model which was 13. This suggests that interpretations of the solar wind velocity correlations are less certain when many lags of V are included. When only one lag is chosen, we avoid this problem. In the multivariable models, Ey, and -VBs were dropped from the analyses because of multicollinearity. When either Ey or -VBs were included, V had VIF values greater than 20. Similarly, the strong interdependence of N with pressure resulted in VIF values of both N and pressure being greater than 20. For this reason, we include both N and P only in the final model, with N and P at different lags

Statistical analyses were performed in IBM SPSS Statistics, IDL, and MATLAB.

3. Results

3.1 Distributed lag models

Due to high correlations between lags of a single predictor, simple cross correlations may attribute more influence to each lag than is valid. To determine which lags are most important, we perform a series of distributed lag models in which all lags of a given predictor are analyzed simultaneously. Following this, we also introduce an autoregressive (AR) term to account for the high persistence of electron flux.

Single parameter distributed lag models, where lags 0-5 are entered in one multiple regression model but there is no autoregressive (AR) term, show similar patterns to cross correlations found in previous studies (Figure 2, light gray bars). Bar heights show the regression coefficients (not correlations). Peak influence in these non-autoregressive models is at lags 1-2 days but the fall off over time is slow. This is likely to be due to the persistence of relativistic electrons. A predictor at lag 5 days, for example, may have acted on flux 5 days previous. That action is still being seen because once electrons are accelerated, they tend to remain at that energy in the radiation belts.

When the autoregressive term is introduced (Figure 2, bars outlined in black), the response changes markedly. Peak influence for most parameters is then at lag 0-1 days and influence drops off dramatically at longer lags. Where all lags of a predictor are entered simultaneously into a multiple regression model (and the autoregressive flux term is added), ULF Pc5, VLF chorus, number of substorms, and solar wind velocity all correlate positively with all flux channels at lag 1 (predictor measured one day previous to flux) (letter a), although solar wind velocity (V) shows a negative effect at lag 2 (b). Many parameters show a negative influence on flux at lag 0 (nowcast). Lag 2 ULF Pc5 and VLF chorus are more modestly correlated with flux (c), although the lag 2 days influence grows as the lag 1 day influence drops at the higher flux energies (3.5-6.0 and 6.0-7.8 MeV, d), suggesting that it takes an extra day for these mechanisms to produce higher energy electrons. However, the influences of further lags drop off much more quickly than they do in simple cross correlations. Pressure, $|B|$, and number density all show a strong negative effect at lag 0 (presumably due to compression, e) with positive correlation at lags 1 and/or 2 (f). Dst shows a strong negative effect at lag 1 (g), suggesting the action of magnetopause shadowing. However, as will be shown later, this appears not to be the case. The influence of the electric field ($E_y = -V \times B_z$) is very similar to the influence of B_z alone.

For the single predictor, multiple lag regressions of Figure 2, all VIF are less than 3, except for the solar wind velocity (V) regression where VIF is <10 for all lags. This suggests that interpretations of the V regression are less certain, but the variance inflation caused by the high correlation of V with itself on subsequent days is not high enough to warrant correction.

3.2 Multivariable regression models

We further investigate the relative influence of variables by analyzing models with several variables included at a time. This allows a comparison of relative strength of influence, as well as the determination whether certain variables only show correlations with flux because of their association with other variables.

For these analyses, we limit lags to 0-2 as lags>2 in the single variable distributed lag models were less important. We break the variables into two sets: internal and external effects. The internal effects are those parameters thought to have a direct effect on flux, the wave activity (ULF Pc5, VLF chorus, and EMIC), availability of seed electrons, Dst (acting through the "Dst effect"), and solar wind pressure and |B| (which are thought to compress the radiation belts inside the orbit of geosynchronous satellites leading to lower observed flux). External effects are the parameters thought to act indirectly by modulating the internal effects. These include Bz and solar wind velocity and number density (V and N) which introduce driving energy into the magnetosphere, as well as substorms which are dependent on these parameters and may mediate the conversion of this driving energy into wave activity. Models that included pressure, Ey, or -VBs together with N, V, or Bz resulted in high multicollinearity between the variables. We therefore did not include Ey or -VBs in these models, and only included pressure when N and V were not present, or when it was at a different lag from N and V.

3.2.1 Internal effects predictor set

First, we compare effects of internal predictors – those processes that are thought to influence flux directly. This includes the three wave types (ULF Pc5, VLF chorus, and EMIC) as well as the available seed electrons (Figure 3) at lags 0-2 (*s*), as well as pressure and |B|at lag 0 (t) to represent the compression of the magnetosphere. This autoregressive, distributed lag model can be represented as:

$$Log\ Flux_t = b_0 + b_{AR} \times Log\ Flux_{t-1} + b_P \times Pressure_t + b_{|B|} \times |B|_t + \sum_{i\ ULF=0}^{s} b_{i\ ULF} \times ULFPc5_{t-s} + \sum_{i\ Chorus=0}^{s} b_{i\ Chorus} \times Chorus_{t-s} + \sum_{i\ EMIC=0}^{s} b_{i\ EMIC} \times EMIC_{t-s} \qquad (2)$$

The standardized regression coefficients show that ULF Pc5 wave activity increases flux on the same day (lag 0) with less effect on the next day (lag 1) (dark gray bars are statistically significant effects). At a 2 day lag, only the highest energy channel shows a significant increase in flux associated with ULF Pc5 (a). VLF chorus waves increase flux on the same day at the lowest three energies (b), and act positively at all energies at lag 1 (c). Chorus shows no significant influence on flux at lag 2; the effects of VLF chorus do not appear to build up over time to the same extent that the ULF Pc5 effect does. The magnitude of the ULF Pc5 and chorus influences are similar, although ULF Pc 5 dominates on lag 0 day. Conversely, EMIC waves are most negatively influential at lag 1 (d), with their strongest effects at the higher energy levels (e). Their effect is lower in magnitude than ULF Pc5 or VLF chorus. Seed electron flux is most influential at the lower energy channels, with lag 0 being most important at the lowest energy (f), the lag 1 influence rising in importance (g), then seed flux losing influence entirely at the highest energy channel (h).

The negative pressure effect at lag 0 (the compression effect) is similar for all energies, although |B| influence drops off slightly at the highest energies. The "Dst effect", in which particles lose energy and are lost as they move outward when the ring current reduces the magnetic field, appears to act immediately at lag 0 (i) with some influence at lag 2 days (j). The positive coefficient at these lags (0 and 2) means that higher flux occurs with a weaker Dst, lower flux with a stronger Dst, as would be predicted if a stronger ring current leads to adiabatic electron loss. When the Dst is stronger (more negative), the magnetic field is weaker (due to the stronger ring current), and electron energy is reduced. The negative effect of Dst at lag 1 (k) indicates that a stronger (more negative) Dst leads to increased flux. This would contradict the prediction made by the "Dst effect", however, it may be explained as an artifact of Dst's correlation with other processes that raise flux levels at this lag. The lag 0 "Dst effect" is less visible in Figure 2 than in Figure 3. It appears to be more visible when other variables are accounted for as they are in Figure 3.

At lag 1 and 2, the regression coefficients of ULF Pc5, VLF chorus, and EMIC waves, and seed electron flux are similar in direction but with magnitudes about 1/3 – 1/2 of those seen in the single predictor distributed lag models of Figure 2. This indicates that some of the effect of each seen in the single variable model is actually due to these other correlated factors. The pressure and |B| coefficients are nearly the same in both the single variable models and these combined models. Thus, the effect of compression is independent of the other variables at geostationary orbit. The negative effects of ULF Pc5 and VLF chorus at lag 0 seen in the single variable distributed lag models (Figure 2) but not in this internal effects combined model (Figure 3) are likely the result of this compression which has now been accounted for by adding pressure and IMF magnitude (|B|) to the model.

The autoregressive component (lag 1 of relativistic electron flux) was also included in these Figure 3 models, but is not shown in the figures. Its standardized regression coefficient varied from .797-.920.

The fraction of variability in the data explained by a model can be measured by R^2 (the coefficient of determination or prediction efficiency). This is roughly equivalent to the square of the correlation coefficient in simple regression and can be used to compare models (R^2 ranges from 0 to a high of 1). For these internal effects models the R^2 values were: 0.901 (0.7 – 1.8 MeV), 0.901 (1.8 – 3.5 MeV), 0.916 (3.5 – 6.0 MeV), and 0.810 (6.0 – 7.8 MeV). The square roots of these (comparable to correlations) were 0.95, 0.95, 0.96, and 0.90. Even without the introduction of external effects, the correlations of these distributed lag autoregressive models are high.

3.2.2 External effects predictor set

A similar analysis for external effects (Bz, |B|, V, N, substorms, and source electron flux (31.7 keV)) is shown in Figure 4. Bz (percent of hours which are below 0 in a 24 h period) is less influential than the other parameters, but this may be due to the use of hourly averages. The hourly averages may miss the strong and quick southward turns that are thought to influence flux. Compared to the other solar wind parameters (V and N), Bz shows only a moderate influence at lag 0. However, this is not evidence of magnetopause shadowing (a direct effect) as the influence is positive. The positive correlation means that more southward Bz increases flux instead of decreasing it as would be predicted by the magnetopause shadowing hypothesis.

The anticipated negative effect is instead seen in the N and |B| regression coefficients as the arrival of the shock compresses the radiation belts. V is most strongly correlated with flux at lag 1. Correlations of V and N with flux are presumably the result of these parameters driving other processes such as wave generation or intermediaries such as substorms or source electrons. Of these intermediate processes, substorms are more influential than source electron flux. The intermediate substorm effect, however, is generally lower than that of V itself. This suggests that the direct driving of internal effects (wave activity) by V is at least as important as the driving through intermediaries such as substorms.

Initially, we included either the -VBs coupling function or the solar wind electric field (Ey) in these external effects models. However, the variance inflation factor (VIF) of V was >20 in these models, suggesting severe problems of multicollinearity. Multicollinearity was also high when pressure was included. With pressure (a multiplicative factor of N and V) in the model, variance inflation factors of N, V, and pressure were all >10.

The fraction of variation explained by these external effects models was similar to that of the internal effects models: 0.886, 0.895, 0.903, and 0.808 for the four energies, respectively. This would correspond to correlations of 0.94, 0.95, 0.95, and 0.90. Either internal or external effects models, therefore, would provide a similar fit to the data.

Our initial attempt to add Ey and -VBs to the external effects models, which resulted in high multicollinearity, did not result in higher R^2 (coefficient of determination, see above). The R^2 of the autoregressive external effects models without Ey or -VBs ranged from 0.808-0.903. When either -VBs or Ey were added to the models, the R^2 increased, at most, by .001. When we replaced V by either -VBs or Ey, the R^2 dropped to .807-.897 (a drop of .001-.010). Similarly, adding pressure to the external effects models (in addition to N and V) resulted in at most a .006 increase in R^2. Substituting pressure for N and V resulted in an R^2 of .805-.897, a drop of .003-.010. Thus, the parameters derived from other parameters (Ey, -VBs, and pressure) have somewhat less explanatory value than the measured parameters of V, N, and Bz. Additionally, adding these terms derived by multiplying V, N, or Bz results in models with multicollinearity problems. Multiplicative coupling functions such as these postulate a synergistic effect of the measured variables. Pressure, for example, would describe the response of flux to a multiplicative interaction between V and N, while including only V and N in the model describes an additive response of flux to the two variables. We explore these relationships further in the companion paper, but in a model with fewer variables and lags so as to reduce multicollinearity problems.

3.2.3 All parameter regression

The analyses presented in Figures 3 and 4 presume that either the set of waves and seed electrons, or that the set of solar wind parameters, substorms, and source electrons can be used independently to predict high energy electron flux. This may be true if solar wind parameters transfer all the necessary energy to the waves and seed electrons which then drive the high energy electron flux. However, solar wind parameters, substorms, and source electrons may drive more than the processes we study here. This can be tested by including all parameters in the same regression model. This will test what effect each variable has on its own, uncoupled from correlations with the other drivers of flux. The standardized regression coefficients of this model allow us to compare the magnitude of effects (Figure 5).

We use lag 0 pressure and |B| as measures of the compression, as well as lag 0 Dst because it showed the most "Dst effect" in Figure 3. We test the lag 1 of all the other variables. Again, we use an autoregressive term (lag 1 $\log_{10}$ flux) but this is not shown in the figure. Its standardized regression coefficient was between 0.724- 0.892. The R^2 of these models for the four energy channels ranged from

0.817-.905, with the square root of the R^2 (corresponding to a correlation coefficient) therefore ranging from 0.90-0.95.

Pressure and |B| at lag 0 retain their strong influence in these full models, indicating that the temporary reduction in flux measurements that may be due to compression of the radiation belts below the satellites is present at all energy levels, no matter what other explanatory variables are in the model. However, the negative effect of pressure at lag 0 may also include the signature of magnetopause shadowing. We cannot tell if the effect is due to temporary compression of the magnetosphere or if it is more permanent electron loss due to magnetopause shadowing.

The "Dst effect" (Dst at lag 0, thought to be associated with the temporary adiabatic loss of energy in the electrons) loses most of its influence in the full parameter model of Figure 5. It is a significant factor at only one energy level, where it shows less than half the effect of compression. (The Dst coefficients, reflecting lower flux levels, are positive because stronger (negative) Dst results in lower flux.) The "Dst effect", therefore, does not appear to be a major influence on flux levels. Thus, the evidence for the action of the "Dst effect" is weak.

Bz, N, and substorms show similar effects in the full model to those shown in the external effects only model, although the V influence is not significant at the lower three energies. The Bz still has less influence than other variables, substorms still show a strong positive effect, and N shows a negative effect. That substorms continue to correlate with relativistic electron flux suggests that there are further processes they drive that accelerate or transport electrons into geosynchronous orbit.

Source electron flux in the full model only shows a significant negative effect at the highest energy. As we include VLF chorus in this model, which is driven by source electrons, the source electron effect seen in the external effects model (Figure 4) may be completely due to chorus waves driven by the source electrons.

ULF Pc5 and VLF chorus again show similar magnitudes of effect at the three lower energy channels. Although ULF Pc5 shows a strong influence in the internal effects model at the highest energy channel, in the full regression model its influence drops close to zero. The introduction of Bz, V,and substorms into the full model may explain this loss of influence, as this is the energy at which these three parameters show the most influence. This would imply that the stronger correlation of ULF Pc5 with the highest energy flux in the internal effects model is a spurious correlation related to some other process which is driven by Bz, V, and substorms, but which is also highly correlated with ULF Pc5 waves.

The negative EMIC effect increases in influence at higher electron energies. . Seed electron flux is still strongly influential on the lower energy channels but now shows a negative impact at the higher energy levels.

Unstandardized regression coefficients for the model of Figure 5 are reported in Table 1. The unstandardized coefficients could be used in a model to predict flux levels in a novel data set (e.g., see Equation 2). The fraction of variation explained by the model (R^2 or prediction efficiency), its square root (correlation), and the effect of the autoregressive term (relativistic electron flux at lag 1) are also reported.

4. Discussion

There are a variety of proposed mechanisms for acceleration, transport, and loss of relativistic electrons at geosynchronous orbit (Figure 1). Using multiple regression analysis, we have presented a comparison of the strength of several of these proposed processes by investigating the relationship between flux and the combined action of wave activity, pressure, solar wind velocity and number density, magnetic field strength, substorms, and the presence of lower energy electrons. As we analyze these in combination, their relative influences can be directly compared. Our analyses also assess the time scale over which each of these drivers operate, giving insight into whether short or long-acting mechanisms are responsible for observed flux levels.

Because each predictor of relativistic electron flux is correlated with itself from one day to the next, and because the high persistence of flux means that an action by a driver on a previous day will have long lasting effects, a simple cross correlation analysis may not single out the times at which a predictor's action is highest. Adding an autoregressive term (flux one day previous) was even more effective at unmasking the most influential lags of predictors. The high persistence of flux gives the impression that drivers act over many days, but this is an illusion based on the fact that flux levels can remain fairly constant after the initial acceleration. The introduction of the autoregressive term restricts the action of a variable to immediate effects. An additional reason for including the autoregressive term is that a regression model with high autocorrelation in the dependent variable may lead to unreliable statistical tests. The AR term eliminates this problem. An autoregressive-distributed lag model, which is able to analyze each lag separately by combining them into one analysis and account for the persistence of flux, shows that parameter effects are limited, for the most part, to 1-2 days.

Predictors are also correlated with each other and an apparent influence of one variable may only be due to its correlation with another that is the actual driver. Simple correlation includes all these effects in a single number and is thus not very useful at determining which parameter, at which lag, is most influential. Separating lags in the distributed lag models and then separating variables in the combined regression gives the action of each predictor independent of the others and independent of itself at different lags. By using standardized regression coefficients, we can compare the strength of effects between parameters despite different measurement scales.

We attempted, in a preliminary investigation, to use rough time-integrated variables as predictors (i.e., averaging over different numbers of days). We did discover that correlations of these averages ("integrated values") were higher with high energy flux, however, this method resulted in a loss of information about which time lag was most important and therefore, which physical processes might be most important. Although this method has been used previously to create models of the relationship between many variables and flux (Borovsky & Denton, 2014; Borovsky, 2017), we were able to acquire more precise information about the timing of effects with distributed lag models.

We analyzed internal effects using only lags 0-2 (current day to two days previous -- the most significant lags in the single variable models). In this model, ULF Pc5 and VLF chorus waves are hypothesized to accelerate seed electrons, while EMIC wave activity decreases flux through precipitation. Pressure and |B| at lag 0 are added as covariates to account for the temporary drop in observed flux due to the compression of the radiation belts inside the orbits of the geosynchronous satellites. The "Dst effect", where electrons temporarily lose energy adiabatically due to a weaker magnetic field (Li et al., 1997; Kim & Chan, 1997; Onsager et al., 2002) is tested by introducing Dst as a term. All entered variables showed some influence on flux at at least one time lag and energy level, demonstrating that each has an independent influence.

External effects (solar wind velocity, pressure, hours of southward Bz, and average |B|) were tested to determine how the introduction of energy into the magnetosphere correlates with flux. The presumed action of these factors is to increase wave activity either directly (e.g., ULF Pc5 waves by the Kelvin-Helmholtz instability (Claudepierre et al., 2008)) or indirectly (e.g., via enhanced substorm activity which injects source electrons which subsequently drive VLF chorus waves (Meredith et al., 2001; 2003a; Tsurutani & Smith, 1974; Li et al., 2009)).

The fractions of variation in the data explained (R^2) by the separate internal and external effects models were similar to each other, ranging from 0.808 – 0.918 (correlation of 0.90 – 0.96), with the lowest predictive ability from the highest energy flux model. If the goal is merely to provide a reasonably accurate predictive model, either the internal or the external effects models would be excellent candidates. However, the internal effects models presumably give us more information about the physical drivers of flux.

In our final models, we included all internal and external effect predictor sets, as well as intermediary substorms and source electrons, to more completely study the relative influences of each. We presented a model with adiabatic/compression effects at lag 0 and other effects at lag 1 day. The R^2 of these full models ranged from 0.817 to 0.905, the lowest being that for the highest energy electrons (correlations ranged from 0.90 – 0.95). The correlation of the full model was not much higher than that of the internal effects alone models. There would therefore be little reason to use the full model for prediction, but we can derive more information about the relative importance of parameters from combining internal and external effects in one model.

4.2 Effects of waves and seed electrons – internal effect predictor set

4.2.1 ULF Pc5 and VLF chorus enhancement of flux

In previous studies, cross correlations of ULF Pc5 waves with relativistic electron flux give the impression that ULF Pc5 waves have their most influence on relativistic electron flux at a lag of 2-3 days. (Mann et al., 2004; Kozyreva et al., 2007; Lam, 2017; Regi et al., 2015). This would imply that ULF Pc5 waves drive acceleration most effectively through long term processes such as radial diffusion. However, in our single predictor distributed lag-autoregressive models, the ULF Pc5 is markedly more influential at lag 1 (lagged by 1 day) over the other lags. Analyzing the effects of all lags in combination, instead of individually as in cross correlation, shifts the influence toward lag 1, but adding the autoregressive term (electron flux on the previous day) is even more influential at centering the ULF Pc5 effect at lag 1. (The light gray bars of Figure 2 show the distributed lag models without the AR term; the darker bars show the analysis with the AR term added.)

However, although ULF Pc5 waves show a negative effect at lag 0 in the single factor distributed lag models, this disappears when pressure and |B| are added in the combined, internal effects model. The high correlation of ULF Pc5 with compression makes it appear these waves are reducing flux in the single factor models, when it is the hidden variable (compression) that is the actual cause. When the compression reduction is accounted for in the combined model, the positive effects of these waves at lag 0 can be seen. The lower influence of lags 1 and 2 in this combined internal-effects model leads to the conclusion that radial diffusion is not the primary action of ULF Pc5 waves, at least at the lower energies. The increased effect of the later lags at the highest energy level could indicate that radial diffusion is more important at higher energies or that short term acceleration processes continue over time, with electrons first being accelerated into the lower energy ranges and from there to the highest ones. ULF Pc5 waves may drive more than one growth process: short acting acceleration whose effects appear at lag 0 (e.g., nonresonant interactions (Shah et al*.,* 2015; Ukhorskiy et al*.,* 2009; Degeling et al., 2013) or magnetic pumping (Liu et al., 1999)) and a longer acting process which increases flux a day or two later (e.g., radial diffusion (Falthammar, 1965; Elkington et al., 1999; Nakamura et al., 2002; Ukhorskiy et al., 2005; Hudson et al., 2000). There is little evidence for effects beyond this time scale.

We have seen only evidence of flux enhancement by ULF Pc5 waves, although they are predicted to also contribute to electron loss via outward radial diffusion during shock events (Degeling et al., 2008; Loto'aniu et al., 2010; Shprits et al., 2006; Ukhorskiy et al., 2009; Zong et al., 2012; Hudson et al., 2014; Brautigam & Albert, 2000). If ULF Pc5 waves are contributing to loss, this effect is overshadowed by the growth processes in the linear models.

VLF chorus waves also show changes in influence as the model is refined. Cross correlations give the impression that chorus is most influential at lag 2 or 3, but the distributed lag model brings the strongest chorus influence to lag 1 with the AR term making this difference even more dramatic. The negative effect at lag 0 in the distributed lag model is again negated by the addition of the correlated compression terms (pressure and |B|) to the internal effects model. Chorus shows an influence over a broader time period than ULF Pc5 waves, acting over both lag 0 and 1 except at the highest energy. At the lower relativistic energies, acceleration by cyclotron resonance of electrons with chorus appears to act over a longer period of time than the acceleration mechanisms driven by ULF Pc5 waves.

With effects at about the same order of magnitude as ULF Pc5 waves, VLF chorus waves act over lag 0 and 1 in the lower flux energy ranges, but the lag 0 effect drops off in the highest energies. This may be the signature of chorus accelerating electrons to lower energies (0.7-3.5 MeV) quickly, but electrons may only be brought to the highest energy levels if there are midrange electrons available for acceleration. Alternatively, it may be that same day chorus precipitates electrons at the highest energies, as well as accelerating them, with the net effect coming close to zero (Lorentzen et al., 2001; Bortnik & Thorne, 2007; Millan and Thorne 2007; Bortnik et al., 2006; Lam et al., 2010; Hikishima et al., 2010; Orlova & Shprits, 2010).

Superposed epoch analyses using ground data or proxies have suggested an association between ground VLF waves and high energy electron flux (Smith et al., 2004; MacDonald et al., 2008; Li et al., 2015), but our previous multiple regression analysis of various factors found only a weak correlation between ground VLF with high energy electron flux (Simms et al., 2015; 2016). In part, this was due to the attenuation of wave activity reaching the ground in the summer months due to solar irradiation of the ionosphere (Smith et al., 2010). Limiting the ground VLF data to the dawn period improved the correlation somewhat, probably because VLF chorus (a flux enhancer) is more prevalent in the morning and hiss (an electron precipitator) more common in the afternoon and dusk (Simms et al., 2015), but Halley ground VLF did not have as a strong an influence as the ULF Pc5 index. Our present multiple regression analysis uses VLF data from the DEMETER satellite instead of ground data from Halley. Using this more robust measure of wave activity, and while holding other factors constant, we have found a stronger correlation with flux than previously. While our previous work did not support the contention that VLF chorus was as influential on flux as ULF Pc5, the current study shows they have effects of similar magnitude.

Chorus is thought to be generated in two regions by two different processes: 1) within 15° of the magnetic equator due to electron injection from substorms near midnight (Meredith et al., 2001), and 2) at higher latitudes due to wave generation in the horns of the magnetosphere (Tsurutani & Smith, 1977). In the present study, we use DEMETER chorus activity from L4 which is generally above ±40° latitude. This is beyond the ±15° latitude range where equatorially generated chorus is produced. These waves do propagate to higher latitudes (Horne & Thorne, 2003), particularly on the dayside (Meredith et al., 2003b; Li et al., 2009; Bunch et al., 2011), albeit with some attenuation (Bortnik et al., 2007). While our data may be partially incorporating equatorially generated chorus propagated to higher latitudes, it will also contain any chorus generated at that location. It is therefore impossible to tell how much of the chorus effect in our model is from chorus generated at the equator and how much from the higher latitudes. This has implications not only for the degree of chorus influence on electron enhancement, as chorus from these two regions may impact enhancement differently, but also for the influence of indirect substorm driving. Chorus generated at higher latitudes is not thought to be as substorm-dependent, however this thinking is based on the use of the AE index to measure substorm activity (Tsurutani & Smith, 1977). More recent studies have questioned the reliability of AE as a measure of substorm activity (Newell & Gjerloev, 2011). The use of newer measures such as the SuperMAG SME or SME-D indices (Gjerloev, 2012) may provide more evidence of higher latitude chorus dependence on substorms. However, in our model, for the purpose of predicting the level of electron enhancement due to chorus, measurements at high latitude may sufficiently represent equatorial chorus. According to Bortnik et al. (2007), propagation to higher latitudes may be L-dependent, but as we limit chorus to a single L-shell this would not introduce bias. Dayside chorus propagates further than nightside, so limiting our averages to this period increases the amount of chorus activity we pick up. Higher frequencies (>0.5fce) do not propagate beyond 15°, but lower frequencies within our averaging range propagate up to at least 56°. This gives us a reasonable chance of picking up at least some of the signature of equatorial chorus. If we observe this chorus signature without bias due to L, MLT, or frequency, then its weakness relative to other signals (such as ULF Pc5) will not, in theory, affect the ability of regression to compare chorus influences with other parameters.

There is some debate about whether VLF chorus is necessary for flux enhancement. A model using ULF Pc5 wave diffusion to model flux, excluding VLF chorus, showed good agreement with observations (Ozeke et al., 2017), leading to the conclusion that if ULF Pc5 waves alone can adequately explain flux levels then VLF waves do not contribute. However, there is a competing hypothesis that chorus is the primary driver after a depletion event (Jaynes et al., 2015). However, distributed lag models (Figures 2 and 3) show slightly more influence of ULF Pc5 than chorus at lag 1. Both waves play a role with roughly equal influence. Although there may be events where one or the other dominates as the primary cause, in general, the two effects combine to enhance flux. In fact, their combined action may not just be additive but synergistic, with the level of one variable influencing the effects of other variables. This is explored further in a companion paper that focuses on nonlinear effects of these factors (Simms et al., 2018b, submitted (Paper 2)).

4.2.2 Seed Electrons

An available population of seed electrons for acceleration into higher energies was an important parameter at the lowest energies studied, but this effect fell off at the highest energies. This accords with the lower seed-relativistic flux correlations at higher energies found in Van Allen Probes data (Tang et al., 2017). In our results, the lag 0 influence fell off faster than the lag 1 over all energy channels. Electrons are accelerated quickly into the lowest energy ranges, then subsequently accelerated to the next highest energy with each channel drawing its new population from the channels just below. This process takes several days for the highest energy channels and no influence of the seed population can be seen at the highest energy channel within the 2 day window. There is no mechanism that takes seed electrons directly to the highest energy level in this short period of time. This accords with correlations found between Van Allen Probes electron measurements and solar wind parameters (Zhao et al., 2017).

4.2.3 Losses Due to EMIC Waves

EMIC waves have been predicted to have a stronger influence in precipitating electrons >2MeV than those at lower energies due to their matching resonant energy (Bortnik et al., 2006), although it has been suggested that cold dense plasma on the duskside may lower the minimum required energy (Jordanova et al., 2008; Blum et al., 2015). Ukhorskiy et al. (2010) also argue that if the predicted effective frequency range is not restricted to the single wave harmonic at the peak of the power spectral density, EMIC-induced electron scattering could occur down to energies as low as 400 keV within seconds. Hendry et al. (2017) found a majority of EMIC-driven flux-precipitation events do occur below 1 MeV. However, both our single variable distributed lag model and the combined model of internal effects show a greater than three-fold increase in precipitation due to lag 1 EMIC waves at the highest energy compared to the effect on .7-1.8 MeV electrons. Thus, although precipitation due to EMIC waves may act at the lower energies, it is more effective at the higher energies. The lack of correlation of flux with lag 0 EMIC waves suggests that the timescale could be up to a day, not over a matter of seconds as has been predicted. However, as we only use daily averages of flux, it is difficult to determine if this is actually the case. EMIC effects on loss are modest compared to the enhancement effects of VLF chorus and ULF Pc5 waves. In one storm, it was found that EMIC waves only lasted for several hours while chorus waves were present for a full 24 h period. This difference could have accounted for the stronger enhancement effects of chorus over the loss due to EMIC waves in that storm period (Turner et al., 2014), and could explain the greater influence of both chorus and ULF Pc5 in general if EMIC waves tend to be shorter lived. It is possible that the underestimation of EMIC wave occurrence by ground stations (Keika et al., 2013; Saikin et al., 2015) might make comparisons of satellite observed chorus effects to ground EMIC influence difficult (Engebretson et al., 2008). As we are comparing daily averaged chorus (and ULF Pc5) waves to all-day occurrence rates of EMIC waves this problem is less severe. Although this may mean that our estimate of EMIC effectiveness is low, it will still have the correct sign.

It should be noted that correlations of EMIC waves with flux show a positive association when the autoregressive term is not present in the model. We suspect this is a consequence of EMIC waves being correlated with other processes that enhance flux. Thus, the negative effects of EMIC waves are only seen in correlation analysis when other factors are accounted for. In particular, we see the negative EMIC influence uncovered even when the only other factor added is the previous day's flux in the single factor distributed lag models.

4.3 Adiabatic and compression effects

The wave effects described above are non-adiabatic enhancement and loss processes. We have also included measures of adiabatic processes in our models: solar wind pressure, magnitude of B, and Dst. Even if we were not interested in the effects of adiabatic processes, it would be important to include them as covariate factors in the analysis of wave effects.

Solar wind pressure, |B|, and the ring current influences are related to changes in compression and magnetic activity. These factors are also highly correlated with the level of magnetospheric activity, which in turn may lead to increased wave activity. Not including these factors could lead to confusion about which process is driving enhancement and loss. Their inclusion also allows an assessment of the relative influence of adiabatic vs non-adiabatic effects (i.e., temporary vs. permanent, long-lived effects).

Solar wind pressure and |B|at lag 0 show a strong negative influence in the single predictor models, as well as in the internal effects model. The simultaneous net effect, during periods of higher solar activity when these factors are high, is that electrons are rapidly depleted at geosynchronous orbit by the arrival of a pressure pulse, while the increased ring current (reduced magnetic field) allows particles to drift outwards and thus, adiabatically, lose energy (Kim & Chan, 1997). While |B| has been predicted to increase flux due to induced electric fields (Foster et al., 2015), at lag 0, the effect of |B| is negative and likely due to an association with compression, similar to the negative pressure effect. The negative correlation of N with flux is also unexpected, although it may also be an indication that number density is strongly associated with compression.

Dst, which measures the ring current and the tendency of electrons to drift outward and lose energy adiabatically, shows a similar lag 0 effect in models where variables are combined. It appears as a positive correlation because stronger Dst is more negative. This is likely due to the high correlation of Dst with positive drivers of flux such as VLF chorus and ULF Pc5 waves. The "Dst effect", in which flux is reduced when lower magnetic field strength allows particles to move outward and adiabatically lose energy (Li et al., 1997; Kim & Chan, 1997; Onsager et al., 2002), is seen in the internal effects model correlations at lag 0 and 2 in the three lower energies. The lower flux is a positive correlation because more negative (stronger) Dst leads to lower flux. However, in the full model (both internal and external effects combined) a Dst effect at lag 1 is only significant for the midrange energies. The rest of the significant effects of Dst appear to be explained by its upstream association with wave activity. Substorms are thought to be associated with moving the trapping boundary inward and thus reducing flux at geosynchronous orbit (Li et al., 1997). Although we found negative correlations between substorms and flux at lag 0 (the same day) in the single variable model, these may be related to the correlated compression effects. Significant negative correlations in the multivariable external effects models only occurred at lag 2. This was two days later than flux reductions associated with compression due to pressure or |B|. The negative effect of the movement of the boundary may be comparatively weak, or delayed, or the effect of substorms on increasing the direct drivers of flux (e.g., VLF chorus, ULF Pc5 waves) outweighs the reductions caused by changes in the trapping boundary. More significant to the question of wave effects, additions of pressure, |B|, and Dst to the internal effects model result in a reversal of the apparent negative correlation of both ULF Pc5 and VLF chorus. While both these wave types showed a negative lag 0 correlation with flux in the single variable distributed lag models, they show a positive effect in the model incorporating pressure pulses, B field magnitude increases, and Dst effects. Pressure and increased magnetic field not only compress the radiation belts, they also mark the increased geomagnetic activity that drives ULF Pc5 and chorus waves. A compression event and/or an increase in ring current are likely to be accompanied by increased wave activity. This correlation of factors (compression, strong Dst, and wave activity) gives the appearance of a negative effect of these waves if compression and Dst are not included in the model as covariates. By adding compression and Dst covariates, the positive influence of ULF Pc5 and chorus activity is unmasked. The negative correlation of these waves with flux seen in the single variable models is only an artifact of not accounting for the large adiabatic and temporary loss due to compression.

Compression of the magnetopause may also produce magnetopause shadowing, where trapped particles cross the magnetopause and are permanently lost (Onsager et al., 2002; Yu et al., 2013; Herrera et al., 2016; Xiang et al., 2017). Losses due to magnetopause shadowing may be considerable and higher than enhancement due to wave acceleration in some storms (Turner et al., 2014). However, it is possible that compression might also result in temporary reduction in electron flux at geosynchronous satellites if the satellites are left outside the magnetosphere during a compression event (Dmitriev et al., 2014). In our statistical analyses, we cannot tell whether losses associated with pressure are permanent, and therefore due to the accepted magnetopause shadowing effect, or temporary due to the radiation belts dipping below the altitude of the satellites.

Magnetic shock events (increased |B|) can also produce electric fields which accelerate electrons (Foster et al., 2015). In our analyses (external effects model), this enhancement occurs at lag 1, with more influence in the lower energy channels. Previous observations of enhancement by electric fields showed a prompt response (< 20 min) (Foster et al., 2015). However, in our statistical study, these rapid enhancement effects are overshadowed by the negative effects of magnetosphere compression at lag 0.

4.4 Drivers of wave activity and the seed electron population

We have already noted how some factors may show a correlation with flux merely because they are associated with the higher wave activity which drives flux during periods of general high geomagnetic activity. However, some factors are thought to specifically drive flux-enhancing wave activity or produce the seed electrons that are accelerated to higher energies. These indirect drivers of flux include substorms, source electrons, southward Bz, and solar wind velocity and number density. In Figure 4 we define these as external effects, although the definition of internal and external is not strict. While pressure and |B| may act directly on measured flux via compression of the radiation belts inside the satellite orbits, and Bz may be associated with magnetopause shadowing, Bz, V, and number density are thought to affect flux indirectly by increasing the wave activity that drives flux acceleration and loss. This indirect influence is thought to be mediated by substorms and source electrons. Of these two presumed intermediate processes, substorms show more positive influence than source electron flux.

We have found that if the Bz is southward during a higher percentage of hours (in 24 h) there can be a moderate increase in flux. At lag 1, this is only seen at the highest flux energy. However, a negative influence is seen in other studies (Yuan & Zong, 2013; Ni et al., 2016), possibly because they include only disturbed periods during storms or strong pressure pulses, or because only strong dropout events are included in the analysis (Boynton et al., 2016). During dropout events, southward Bz results in injection of ions which are presumed to increase EMIC wave activity which subsequently leads to further high energy electron flux decreases (Gao et al., 2015). In this scenario, southward Bz acts only in an indirect manner, via increased EMIC wave activity. However, our results suggest that a southward Bz may also result in enhancement. Enhancement could also occur indirectly, via Injection of source energy electrons (<100 keV) which lead to increased VLF chorus wave activity which drives high energy electron fluxes (Jaynes et al., 2015). In addition, periods of southward Bz bring an influx of seed electrons (hundreds of keV) to geosynchronous orbit which would also lead to increased high energy electron flux (Kress et al., 2014).

High speed solar wind is thought to drive ULF Pc5 waves through the Kelvin-Helmholtz instability (Rae et al., 2005). As a consequence, solar wind velocity should correlate well with electrons that have been enhanced by ULF Pc5 activity which is itself ultimately driven by solar wind velocity (Kavosi & Raeder, 2015). Not only that, but including these waves in the regression model (the full model) should cause the V influence to drop out if its entire influence is mediated through the ULF Pc5 waves. For the lower three energies, this is true. However, velocity shows a strong correlation with flux at the highest energy level even when ULF Pc5 is accounted for in the full model (Figure 5). This suggests either that velocity directly drives high energy electron flux enhancement through undetermined processes, or, more likely, that it is responsible for driving another flux-enhancing wave that acts most strongly on the highest energy electrons – a wave type that we have not included in our model.

Previous cross correlational studies have found the highest correlation between solar wind velocity and flux at lag 2 (Paulikas & Blake, 1979; Sakaguchi et al., 2013; Zhao et al., 2017), however our distributed lag models (where several lags of V are entered simultaneously) show that the correlation with velocity is highest at lag 1. The high correlation seen at lag 2 in previous cross correlation analyses is inflated by the high correlation between lags. Our result shows that velocity acts more quickly. By lag 2, in fact, the velocity effect is actually negative.

At lag 1, we attempted to add several coupling functions to the models: pressure, -VBs, and Ey. However, as all three are derived from multiplying V with either N or Bz (or Bz<0), each of these coupling functions is highly correlated with the main effects of V, N, or Bz already present. The multicollinearity in such a model (as measured by the variance inflation factor) was high enough that the resulting model would likely not be a good predictor using novel data. Their addition did not appreciably raise the ability of the model to explain variation in the existing data (as measured by R^2), and substituting the coupling functions for the main effects of V, N, and Bz resulted in models with lower R^2. Due to the multicollinearity issues, we do not feel adding the lag 1 multiplicative terms would result in a stable model for predictive purposes and use only the lag 0 of pressure in the full model, which produced less multicollinearity with the lag 1 V and N terms. However, these coupling functions could describe a multiplicative (synergistic) action, while the addition of the main effects individually describes only the additive relationship. Although incorporating both multiplicative and additive terms in a single model may result in multicollinearity (and possibly a less stable model) the simultaneous testing of them can provide information about their joint action. For this reason, we explore the multiplicative relationship further for pressure in our companion paper (Simms et al., 2018b).

Substorms are thought to play several roles in controlling flux levels: providing source electrons (several - 100keV) whose anisotropies drive flux-enhancing VLF chorus waves, injecting seed electrons (several hundreds of keV) that are accelerated to relativistic energies, and creating localized magnetic field line stretching which can lead to electron dropouts. Our analyses report mostly positive correlations of flux with substorms. The negative correlation at lag 0 of the distributed lag (single predictor) model could be solely due to correlation with the strong effects of pressure and B magnitude much as the V, ULF Pc5, and VLF chorus are.

Previous work has found the peak enhancement of flux by substorms (as measured by AL) to occur at lag 1, with still significant enhancement at lag 2 (Zhao et al., 2017). We see this same pattern in our simple correlations, but multiple regression including other solar wind parameters (external effects model) shows a strong lag 0 effect at lower energies, transitioning to a stronger positive lag 2 effect only at the higher energies. Substorms represent a number of processes and are themselves driven by solar wind velocity, pressure, and Bz. Including several of these other variables in the analysis should reduce the substorm effect, or at least change its time of action. For example, the inclusion of substorm-driven source electrons could be expected to cause the substorm effect to drop out entirely, if the injection of source electrons was a substorm's only contribution to flux enhancement. However, not only is there is still a positive substorm correlation when seed and source electrons are accounted for in the analysis, at the highest energy levels this correlation is as large or larger than any other effect. This suggests either that processes associated with substorms that we have not included also drive acceleration, or that substorms inject high energy electrons along with the seed and source electrons. Other studies have shown injection of MeV electrons by dipolarization during substorms at geosynchronous orbit or just below (Ingraham et al., 2001; Dai et al., 2014, 2015; Tang et al., 2016). Our regression model, comparing enhancement effects, shows that substorm injections of MeV electrons are at least as important as wave acceleration in the higher energy channels.

Source electrons with energies in the tens of keV (31.7 keV in our models) have been observed driving VLF chorus waves which then act to accelerate seed electrons (Reeves et al., 2013; Baker et al., 2014; Foster et al., 2015). As expected, seed electrons (270 keV in our models) show positive correlations with high electron energy flux, at least at the lower energy channels. As noted above, the fall off in correlation at the highest energy levels may be a consequence of seed electrons not being accelerated directly to these highest energies. This is also consistent with the first enhancements appearing in the 10-100 keV electron population, followed by later enhancements of the higher energy electron populations (Boyd et al., 2014; 2016). Source electrons (31.7 keV), however, tend to show negative or no correlation at lag 0 and 1 in the multivariable models, despite their strong correlations with flux seen in the simple correlations of Figure 2. The loss of source electron influence in the multivariable models suggests that they only drive flux indirectly. Presumably, this is through their driving of VLF chorus waves, which subsequently drive flux. Once VLF chorus is added to the model, the source electron correlation with flux is already explained and the source electron effect drops out.

4.5 Complexity of the system

The complexity of the system is demonstrated by the intricate balance of changing effects as different variables are added to the models. Most notably, the strong effect of ULF Pc5 seen in the internal effects model at high energy (Figure 3) drops out in the full regression (Figure 5). This is most likely due to the addition of V or substorms, which show a strong influence on the highest energy channel. The ULF Pc5 correlation with flux in the internal effects model is most likely due to the hidden correlation of ULF Pc5 with these influential factors. In a similar fashion, the drop in source electron flux influence is likely due to the addition of VLF chorus waves to the full model. In this case, we can draw the conclusion that source electrons are no longer influential on high energy electron flux when the chorus waves that they drive (which subsequently accelerate electrons to high energies) are also included in the analysis.

5. Summary

1. Multiple regression allows a direct comparison of influences on relativistic electrons at geosynchronous orbit, while accounting for the effects of other variables. With this technique we are able to determine which factors are the strongest influences, and which only appear influential due to their correlation with the driving parameters. This potentially provides more information than would be obtained from a neural network analysis. As all parameters are tested simultaneously their relative influences within the model can be directly compared via the standardized regression coefficients. We introduce an autoregressive term (flux on the previous day) to improve robustness of statistical tests. This has the added benefit of testing influences of parameters without the confounding influence of flux persistence. In addition to this, distributed lag models allow the testing of each predictor lag, while accounting for the influence of the same predictor at other lags. This allows us to determine at which lag physical effects of these predictors are acting and is thus an improvement over time-integrated correlations which combine several lags together.

2. We analyze internal effects (waves, seed electrons, and compression) separately from external effects (solar wind influences and substorms), to determine relative influences of direct drivers without confusing influences between these sets. Much of the variation in high energy electron flux can be explained by the internal drivers without the inclusion of external drivers in the model. A final combined analysis of internal and external effects confirms this, with internal drivers showing more consistently statistically significant influence than the solar wind external drivers. Substorms and velocity, however, show influence at the highest energy electrons even when wave influences are accounted for. This suggests either another unaccounted process driven by them (likely in the case of V), or that they are directly responsible for enhancements (by direct injection as may be the case with substorms). These combined autoregressive analyses result in predictive models that explain 81.7 – 90.5 % of the variation in the data ($r = .904 - .951$).

3. ULF Pc5 and VLF chorus waves have approximately the same magnitude of influence on $\log_{10}$ relativistic electron flux at the two lower energy channels (0.7 – 3.5 MeV). At higher flux energies, the chorus influence remains strong while the ULF Pc5 influence drops off. Loss due to EMIC waves is less influential, and only significant at the higher flux energies.

4. Injection of high energy electrons by substorms is at least as important as acceleration by wave action at some energies. At the highest flux energies it dominates over wave influences.

5. The "Dst effect" -- a decrease in flux seen during the main phase of storms -- is not generally a significant effect when pressure and $|B|$ are included in the model.

6. A distributed lag model allows a comparison of a variable's effect at different times. Although simple cross correlation suggests that parameters have an appreciable influence up to 5 days later, the distributed lag models show that this is limited to 0-2 days.

7. Accounting for compression which results in magnetopause shadowing removes the negative correlation seen in most variables in the distributed lag models at day 0. The compression effects accounted for by solar wind pressure and |B| are strong and consistent over the four energy channels.

8. Although previous studies have found strong flux enhancement related to more southward Bz, we have found that the magnitude of this influence is less than that seen from ULF Pc5 and VLF chorus waves, solar wind velocity, presence of seed electrons, or substorms. Although southward Bz shows some independent influence, its strong effects seen in other studies are likely because it is a marker for these other processes, rather than that it is a major influence itself.

9. Simple coupling functions such as Ey or -VBs do not provide more predictive information (as measured by R^2) about solar wind influences than multiple regression incorporating the measured parameters (V and Bz) as separate main effects.

Acknowledgements

We thank J. Bortnik and Y. Shprits for their comments on a previous draft of this work, M. Ohnsted and N. Capman for EMIC wave identification, and R. Gamble for preparing and J.-J. Berthelier for providing DEMETER ICE data. Relativistic, seed, and source electron flux data were obtained from Los Alamos National Laboratory (LANL) geosynchronous energetic particle instruments (contact: G. D. Reeves). The ULF Pc5 index is available at http://ULF Pc5.gcras.ru/. The substorm list is available from SuperMAG (http://supermag.jhuapl.edu/ , Principal Investigator Jesper Gjerloev), derived from magnetometer data from Intermagnet; USGS, Jeffrey J. Love; CARISMA, PI Ian Mann; CANMOS; The S-RAMP Database, PI K. Yumoto and Dr. K. Shiokawa; The SPIDR database; AARI, PI Oleg Troshichev; The MACCS program, PI M. Engebretson, Geomagnetism Unit of the Geological Survey of Canada; GIMA; MEASURE, UCLA IGPP and Florida Institute of Technology; SAMBA, PI Eftyhia Zesta; 210 Chain, PI K. Yumoto; SAMNET, PI Farideh Honary; The institutes who maintain the IMAGE magnetometer array, PI Eija Tanskanen; PENGUIN; AUTUMN, PI Martin Connors; DTU Space, PI Dr. Rico Behlke; South Pole and McMurdo Magnetometer, PI's Louis J. Lanzarotti and Alan T. Weatherwax; ICESTAR; RAPIDMAG; PENGUIn; British Artarctic Survey; McMac, PI Dr. Peter Chi; BGS, PI Dr. Susan Macmillan; Pushkov Institute of Terrestrial Magnetism, Ionosphere and Radio Wave Propagation (IZMIRAN); GFZ, PI Dr. Juergen Matzka; MFGI, PI B. Heilig; IGFPAS, PI J. Reda; University of L'Aquila, PI M. Vellante. IMF Bz, Dst, and solar wind V, N, and P data are available from Goddard Space Flight Center Space Physics Data Facility at the OMNIWeb data website (http://omniweb.gsfc.nasa.gov/html/ow_data.html). Work at Augsburg University was supported by NSF grants AGS-1264146, PLR-1341493, and AGS- 1651263.

References

Albert, J. M. (2003), Evaluation of quasi-linear diffusion coefficients for EMIC waves in a multispecies plasma, J. Geophys. Res., 108, NO. A6, 1249, doi:10.1029/2002JA009792.

Almon, S. (1965), The distributed lag between capital appropriations and expenditures, Econometrica, Vol. 33, No. 1 (Jan.,1965), pp. 178-196.

Anderson, R. R. and K. Maeda (1977), VLF emissions associated with enhanced magnetospheric electrons, J. Geophys. Res., 82, 135-146, doi: 10.1029/JA082i001p00135.

Anderson, B.J. and D.C. Hamilton (1993), Electromagnetic ion cyclotron waves stimulated by modest magnetospheric compressions, J. Geophys. Res., 98, PAGES1 1,369-11,38, doi: 10.1029/93JA00605.

Baker, D.N., S. G. Kanekal, X. Li, S. P. Monk, J. Goldstein and J. L. Burch (2004) Nature 432, 878–881, doi:10.1038/nature03116.

Baker, D. N., et al. (2014), Gradual diffusion and punctuated phase space density enhancements of highly relativistic electrons: Van Allen Probes observations, Geophys. Res. Lett., 41, 1351–1358, doi:10.1002/2013GL058942.

Berthelier, J.J., M. Godefroy, F. Leblanc, M. Malingre, M. Menvielle, D. Lagoutte, J.Y. Brochot, F. Colin, F. Elie, C. Legendre, P. Zamora, D. Benoist, Y. Chapuis, J. Artru, R. Pfaff (2006), ICE, the electric field experiment on DEMETER, Planetary and Space Science 54, 456–471, doi:10.1016/j.pss.2005.10.016.

Blum, L. W., E. A. MacDonald, S. P. Gary, M. F. Thomsen, and H. E. Spence (2009), Ion observations from geosynchronous orbit as a proxy for ion cyclotron wave growth during storm times, J. Geophys. Res., 114, A10214, doi:10.1029/2009JA014396.

Blum, L. W., et al. (2015), Observations of coincident EMIC wave activity and duskside energetic electron precipitation on 18–19 January 2013, Geophys. Res.Lett., 42, 5727–5735, doi:10.1002/2015GL065245.

Borovsky, J. E. (2017). Time-integral correlations of multiple variableswith the relativistic-electron flux atgeosynchronous orbit: The strong roles of substorm-injected electrons and the ion plasma sheet. Journal of Geophysical Research: Space Physics, 122,11,961–11,990. https://doi.org/10.1002/2017JA024476.

Borovsky, J. E. and M. H. Denton (2014), Exploring the cross correlations and autocorrelations of the ULF Pc5 indices and incorporating the ULF Pc5 indices into the systems science of the solar wind-driven magnetosphere, J. Geophys. Res., 10.1002/2014JA019876.

Bortnik, J., R. M. Thorne, T. P. O'Brien, J. C. Green, R. J. Strangeway, Y. Y. Shprits, and D. N. Baker (2006), Observation of two distinct, rapid loss mechanisms during the 20 November 2003 radiation belt dropout event, J. Geophys. Res., 111, A12216, doi:10.1029/2006JA011802.

Bortnik, J. and R.M. Thorne (2007), The dual role of ELF/VLF chorus waves in the acceleration and precipitation of radiation belt electrons, J. Atmos. Solar-Terr. Phys., 69 (2007) 378–386, doi:10.1016/j.jastp.2006.05.030.

Bortnik, J., R. M. Thorne, and N. P. Meredith (2007), Modeling the propagation characteristics of chorus using CRRES suprathermal electron fluxes, J. Geophys. Res., 112, A08204, doi:10.1029/2006JA012237.

Boyd, A. J., H. E. Spence, S. G. Claudepierre, J. F. Fennell, J. B. Blake, D. N. Baker, G. D. Reeves, and D. L. Turner (2014), Quantifying the radiation belt seed population in the March 17, 2013 electron acceleration event, Geophys. Res. Lett., 41, 2275–2281, doi:10.1002/2014GL059626.

Boyd, A. J., H. E. Spence, C.-L. Huang,G. D. Reeves, D. N. Baker, D. L. Turner,S. G. Claudepierre, J. F. Fennell,J. B. Blake, and Y. Y. Shprits (2016),Statistical properties of theradiation belt seed population, J. Geophys. Res. Space Physics, 121, 7636–7646, doi:10.1002/2016JA022652.

Boynton, R. J., M. A. Balikhin, S. A. Billings, G. D. Reeves, N. Ganushkina, M. Gedalin, O. A. Amariutei, J. E. Borovsky, and S. N. Walker (2013), The analysis of electron fluxes at geosynchronous orbit employing a NARMAX approach, J. Geophys. Res. Space Physics, 118, 1500–1513, doi:10.1002/jgra.50192.

Boynton, R. J., D. Mourenas, and M. A. Balikhin (2016), Electron flux dropouts at Geostationary Earth Orbit: Occurrences, magnitudes, and main driving factors, J. Geophys. Res. Space Physics, 121, 8448–8461, doi:10.1002/2016JA022916.

Brautigam, D. H. and J.M. Albert (2000), Radial diffusion analysis of outer radiation belt electrons during the October 9, 1990, magnetic storm, J. Geophys. Res., 105, 291-309, doi: 10.1029/1999JA900344.

Bunch, N. L., M. Spasojevic, and Y. Y. Shprits (2011), On the latitudinal extent of chorus emissions as observed by the Polar Plasma Wave Instrument, J. Geophys. Res., 116, A04204, doi:10.1029/2010JA016181.

Cahill, Jr. L. J., N. G. Lin, J. H. Waite, M. J. Engebretson, and M. Sugiura (1990), Toroidal Standing Waves Excited by a Storm Sudden Commencement: DE 1 Observations, J. Geophys. Res., 95, NO. A6, PAGES 7857-7867, doi: 10.1029/JA095iA06p07857.

Chen, Y., Friedel, R. H. W., and G. D. Reeves (2006), Phase space density distributions of energetic electrons in the outer radiation belt during two Geospace Environment Modeling Inner Magnetosphere/Storms selected storms, J. Geophys. Res., 111, A11S04, doi:10.1029/2006JA011703.

Claudepierre, S. G., S. R. Elkington, and M. Wiltberger (2008), Solar wind driving of magnetospheric ULF Pc5 waves: Pulsations driven by velocity shear at the magnetopause, J. Geophys. Res., 113, A05218, doi:10.1029/2007JA012890.

Clausen, L.B.N., J.B.H. Baker, J.M.Ruohoniemi, and H.J. Singer (2011a), ULF Pc5 wave characteristics at geosynchronous orbit during the recovery phase of geomagnetic storms associated with strong electron acceleration, J. Geophys. Res., 116, A09203, doi:10.1029/2011JA016666.

Clausen, L. B. N., J. B. H. Baker, J. M. Ruohoniemi, and H. J. Singer (2011b), EMIC waves observed at geosynchronous orbit during solar minimum: Statistics and excitation, J. Geophys. Res., doi: 10.1029/2011JA016823.

Clilverd, Mark A., Craig J. Rodger, Robyn M. Millan, John G. Sample, Michael Kokorowski, Michael P. McCarthy, Thomas Ulich, Tero Raita, Andrew J. Kavanagh, and Emma Spanswick (2007), Energetic particle precipitation into the middle atmosphere

triggered by a coronal mass ejection, J. Geophys. Res., 112, A12206, doi:10.1029/2007JA012395.

Clilverd, M. A., R. Duthie, R. Hardman, A. T. Hendry, C. J. Rodger, T. Raita, M. Engebretson, M. R. Lessard, D. Danskin, and D. K. Milling (2015), Electron precipitation from EMIC waves: A case study from 31 May 2013, J. Geophys. Res. Space Physics, 120, 3618–3631, doi:10.1002/2015JA021090.

Dai, L., J. R. Wygant, C. A. Cattell, S. Thaller, K. Kersten, A. Breneman, X. Tang, R. H. Friedel, S. G. Claudepierre, and X. Tao (2014), Evidence for injection of relativistic electrons into the Earth's outer radiation belt via intense substorm electric fields, Geophys. Res. Lett., 41, 1133–1141, doi:10.1002/2014GL059228.

Dai, L., et al. (2015), Near-Earth injection of MeV electrons associated with intense depolarization electric fields: Van Allen Probes observations, Geophys. Res. Lett., 42, 6170–6179, doi:10.1002/2015GL064955.

Degeling, A. W., L. G. Ozeke, R. Rankin, I. R. Mann, and K. Kabin (2008), Drift resonant generation of peaked relativistic electron distributions by Pc 5 ULF Pc5 waves, J. Geophys. Res., 113, A02208, doi:10.1029/2007JA012411.

Degeling, A.W., R. Rankin, K. Murphy, and I.J. Rae (2013), Magnetospheric convection and magnetopause shadowing effects in ULF Pc5 wave-driven energetic electron transport, J. Geophys. Res. Space, 118, 2919–2927, doi:10.1002/jgra.50219.

Degeling, A. W., R. Rankin, and Q.-G. Zong (2014), Modeling radiation belt electron acceleration by ULF Pc5 fast mode waves, launched by solar wind dynamic pressure fluctuations, J. Geophys. Res. Space Physics, 119, 8916–8928, doi:10.1002/2013JA019672.

Degtyarev, V.I., I.P. Kharchenko, A.S. Potapov, B. Tsegmed, and S.E. Chudnenko (2009), Qualitative estimation of magnetic storm efficiency in producing relativistic electron flux in the Earth's outer radiation belt using geomagnetic pulsations data, Advances in Space Research, 43, 829–836, doi:10.1016/j.asr.2008.07.004.

S. Derksen and H. J. Keselman (1992). Backward, forward and stepwise automated subset selection algorithms: Frequency of obtaining authentic and noise variables, British J Math Stat Psych 45, pp. 265–282.

Dmitriev, A. V., A. V. Suvorova, J.-K. Chao, C. B. Wang, L. Rastaetter, M. I. Panasyuk, L. L. Lazutin, A. S. Kovtyukh, I. S. Veselovsky, and I. N. Myagkova (2014), Anomalous dynamics of the extremely compressed magnetosphere during 21 January 2005 magnetic storm, J. Geophys. Res. Space Physics, 119, 877–896, doi:10.1002/ 2013JA019534.

Drozdov, A. Y., Y. Y. Shprits, M. E. Usanova, N. A. Aseev, A. C. Kellerman, and H. Zhu (2017), EMIC wave parameterization in the long-term VERB code simulation, J. Geophys. Res. Space Physics, 122, 8488–8501, doi:10.1002/2017JA024389.

Elkington, S.R, M.K Hudson, and A.A. Chan (1999), Acceleration of relativistic electrons via drift-resonance interaction with toroidal-mode Pc5 oscillations, Geophys. Res. Lett., 26, 3273, 10.1029/1999GL003659.

Elkington, S.R., M.K. Hudson, and A.A.Chan (2003), Resonant acceleration and diffusion of outer zone electrons in an asymmetric geomagnetic field, J. Geophys. Res., 108, NO. A3, 1116, doi:10.1029/2001JA009202.

Engebretson, M. J., et al. (2008), Pc1– Pc2 waves and energetic particle precipitation during and after magnetic storms: Superposed epoch analysis and case studies, J. Geophys. Res., 113, A01211, doi:10.1029/2007JA012362.

Engebretson, M. J., J. L. Posch, J. R. Wygant, C. A. Kletzing, M. R. Lessard, C.-L. Huang, H. E.Spence, C. W. Smith, H. J. Singer, Y. Omura, R. B. Horne, G. D. Reeves, D. N. Baker, M. Gkioulidou, K. Oksavik, I. R. Mann, T . Raita, and K. Shiokawa (2015), Van Allen probes, NOAA, GOES, and ground observations of an intense EMIC wave event extending over 12 h in magnetic local time, J. Geophys. Res. Space Physics, 120, doi:10.1002/2015JA021227.

Erlandson, R.E. and A.J. Ukhorskiy (2001), Observations of electromagnetic ion cyclotron waves during geomagnetic storms: Wave occurrence and pitch angle scattering, J. Geophys. Res., 106, NO. A3, PAGES 3883-3895, doi: 10.1029/2000JA000083.

Falthammar, C.-G. (1965), Effects of time-dependent electric fields on geomagnetically trapped radiation, J. Geophys. Res., 70, 2503-2516, 10.1029/JZ070i011p02503.

Forsyth, C., et al. (2016), What effect do substorms have on the content of the radiation belts?, J. Geophys. Res. Space Physics, 121, doi:10.1002/2016JA022620.

Foster, J. C., J. R. Wygant, M. K. Hudson, A. J. Boyd, D. N. Baker, P. J. Erickson, and H. E. Spence (2015), Shock-induced prompt relativistic electron acceleration in the inner magnetosphere, J. Geophys. Res. Space Physics, 120, 1661–1674, doi:10.1002/2014JA020642.

Fraser, B. J., R. S. Grew, S. K. Morley, J. C. Green, H. J. Singer, T. M. Loto'aniu, and M. F. Thomsen (2010), Storm time observations of electromagnetic ion cyclotron waves at geosynchronous orbit: GOES results, J. Geophys. Res., 115, A05208, doi:10.1029/2009JA014516.

Gao, X., W. Li, J. Bortnik, R. M. Thorne, Q. Lu, Q. Ma, X. Tao, and S. Wang (2015), The effect of different solar wind parameters upon significant relativistic electron flux dropouts in the magnetosphere, J. Geophys. Res. Space Physics, 120,4324–4337, doi:10.1002/2015JA021182.

Gjerloev, J. W. (2012), The SuperMAG data processing technique, J. Geophys. Res., 117, A09213, doi:10.1029/2012JA017683.

Halford, A. J., B. J. Fraser, and S. K. Morley (2010), EMIC wave activity during geomagnetic storm and nonstorm periods: CRRES results, J. Geophys. Res., 115, A12248, doi:10.1029/2010JA015716.

Halford, A. J., et al. (2015), BARREL observations of an ICME-shock impact with the magnetosphere and the resultant radiation belt electron loss, J. Geophys. Res. Space Physics, 120, 2557–2570, doi:10.1002/2014JA020873.

Harrell, F. E. (2015), Regression modeling strategies: With applications to linear models, logistic regression, and survival analysis, Springer-Verlag, New York.

Hendry, A. T., C. J. Rodger, M. A. Clilverd, N. R. Thomson, S. K. Morley, and T. Raita (2012), Rapid radiation belt losses occurring during high speed solar wind stream driven storms: Importance of energetic electron precipitation, in Dynamics of the Earth's Radiation Belts and Inner Magnetosphere, Geophys. Monogr. Ser., vol. 199, edited by D. Summers et al., pp. 213–223, AGU, Washington, D. C., doi:10.1029/ 2012GM001299.

Hendry, A. T., C. J. Rodger, and M. A. Clilverd (2017), Evidence of sub-MeV EMIC-driven electron precipitation, Geophys. Res. Lett., 44, 1210–1218, doi:10.1002/2016GL071807.

Herrera, D., V. F. Maget, and A. Sicard-Piet (2016), Characterizing magnetopause shadowing effects in the outer electron radiation belt during geomagnetic storms, J. Geophys. Res. Space Physics, 121, 9517–9530, doi:10.1002/2016JA022825.

Hikishima, M., Y. Omura, and D. Summers (2010), Microburst precipitation of energetic electrons associated with chorus wave generation, Geophys. Res. Lett., 37, L07103, doi:10.1029/2010GL042678.

Horne, R. B. and R. M. Thorne (1998), Potential waves for relativistic electron scattering and stochastic acceleration during magnetic storms, Geophys. Res. Lett., 25, 3011–3014, doi: 10.1029/98gl01002.

Horne, R. B., and R. M. Thorne (2003), Relativistic electron acceleration and precipitation during resonant interactions with whistler-mode chorus, Geophys. Res. Lett., 30, 1527, doi:10.1029/2003GL016973, 10.

Horne, R. B., R. M. Thorne, S. A. Glauert, J. M. Albert, N. P. Meredith, and R. R. Anderson (2005a), Timescale for radiation belt electron acceleration by whistler mode chorus waves, J. Geophys. Res., 110, A03225, doi:10.1029/2004JA010811.

Horne, R.B., R. M. Thorne, Y. Y. Shprits, N. P. Meredith, S. A. Glauert, A. J. Smith, S. G. Kanekal, D. N. Baker, M. J. Engebretson, J. L. Posch, M. Spasojevic, U. S. Inan, J. S. Pickett, and P. M. E. Decreau (2005b), A critical test of electron acceleration in the Van Allen radiation belts, Nature, 437(8), 227–230, doi:10.1038/nature03939.

Hudson, M. K., S.R. Elkington, and J.G. Lyon (2000), Increase in relativistic electron flux in the inner magnetosphere: ULF Pc5 wave mode structure, Adv. Space Res., 25, 2327-2337.

Hudson, M. K., D. N. Baker, J. Goldstein, B. T. Kress, J. Paral, F. R. Toffoletto, and M. Wiltberger (2014), Simulated magnetopause losses and Van Allen Probe flux dropouts, Geophys. Res. Lett., 41, 1113–1118, doi:10.1002/2014GL059222.

Hwang, J. A., D.-Y. Lee, L. R. Lyons, A. J. Smith, S. Zou, K. W. Min, K.-H. Kim, Y.-J. Moon, and Y. D. Park (2007), Statistical significance of association between whistler-mode chorus enhancements and enhanced convection periods during highspeed streams, J. Geophys. Res., 112, A09213, doi:10.1029/2007JA012388.

Iles, H.A., N.P. Meredith, A.N. Fazakerley, and R.B. Horne (2006), Phase space density analysis of the outer radiation belt energetic electron dynamics, J. Geophys. Res., 111, A03204, doi:10.1029/2005JA011206.

Ingraham, J.C., T.E. Cayton, R. D. Belian, R. A. ChristensenR, . H. W. Friedel, M. M. Meier, G. D. Reeves, and M. Tuszewski (2001), Substorm injection of relativistic electrons to geosynchronous orbit during the great magnetic storm of March 24, 1991, J. Geophys. Res., 106, PAGES2 5,759-25,776, doi: 10.1029/2000JA000458.

Jaynes, A. N., D.N. Baker, H.J. Singer, J.V. Rodriguez, T.M. Loto'aniu, A. F. Ali, S.R. Elkington, X. Li, S.G. Kanekal, J.F. Fennell, W. Li, R.M. Thorne, C.A. Kletzing, H.E. Spence, and G.D. Reeves (2015), Source and Seed Populations for Relativistic Electrons: Their Roles in Radiation Belt Changes, J. Geophys. Res. Space Physics, 120, 7240–7254, doi:10.1002/2015JA021234.

Jordanova, V. K., J. Albert, and Y. Miyoshi (2008), Relativistic electron precipitation by EMIC waves from self-consistent global simulations, J. Geophys. Res., 113, A00A10, doi:10.1029/2008JA013239.

Kavosi, S. and J. Raeder (2015), Ubiquity of Kelvin–Helmholtz waves at Earth's Magnetopause, Nature Comm., 6:7019, DOI: 10.1038/ncomms8019.

Keika, K., K. Takahashi, A. Y. Ukhorskiy, and Y. Miyoshi (2013), Global characteristics of electromagnetic ion cyclotron waves: Occurrence rate and its storm dependence, J. Geophys.Res. Space Physics, 118, 4135–4150, doi:10.1002/jgra.50385.

Kellerman, A. C., Y. Y. Shprits, and D. L. Turner (2013), A Geosynchronous Radiation-belt Electron Empirical Prediction (GREEP) model, SpaceWeather, *11*, 463–475, doi:10.1002/swe.20074.

Kepko, L., and H. E. Spence (2003), Observations of discrete, global magnetospheric oscillations directly driven by solar wind density variations, J. Geophys. Res., 108(A6), 1257, doi:10.1029/2002JA009676.

Kessel, R. L. (2008), Solar wind excitation of Pc5 fluctuations in the magnetosphere and on the ground, J. Geophys. Res., 113, A04202, doi:10.1029/2007JA012255.

Kim, H.-J. and A. A. Chan (1997), Fully adiabatic changes in storm time relativistic electron fluxes, J. Geophys. Res., doi: 10.1029/97JA01814.

Kissinger, J., L. Kepko, D. N. Baker, S. Kanekal. W. Li, R.L. McPherron, and V. Angelopous (2014), The importance of storm time steady magnetospheric convection in determining the final relativistic electron flux level, J. Geophys. Res. Space Physics, 119, 7433-7443, doi: 10.1002/2013JA019948.

Kozyreva, O., V. Pilipenko, M. J. Engebretson, K. Yumoto, J. Watermann, and N. Romanova (2007), In search of a new ULF Pc5 wave index: Comparison of Pc5 power with dynamics of geostationary relativistic electrons, Planet. Space Sci., 55, 755–769.

Kress, B. T., M. K. Hudson, and J. Paral (2014), Rebuilding of the Earth’s outer electron belt during 8–10 October 2012, Geophys. Res. Lett., 41, 749–754, doi:10.1002/2013GL058588.

Lam, M. M. R. B. Horne, N. P. Meredith, S. A. Glauert, T. Moffat‐Griffin, and J. C. Green (2010), Origin of energetic electron precipitation >30 keV into the atmosphere, J. Geophys. Res., 115, A00F08, doi:10.1029/2009JA014619.

Lam, H.-L. (2017), On the predictive potential of Pc5 ULF waves to forecast relativistic electrons based on their relationships over two solar cycles, Space Weather, 15, 163–179, doi:10.1002/2016SW001492.

Li, L., J. B. Cao, and G. C. Zhou (2005), Combined acceleration of electrons by whistler-mode and compressional ULF Pc5 turbulences near the geosynchronous orbit, J. Geophys. Res, 110, A03203, doi:10.1029/2004JA010628.

Li, L. Y., J. B. Cao, G. C. Zhou, and X. Li (2009), Statistical roles of storms and substorms in changing the entire outer zone relativistic electron population, J. Geophys. Res., 114, A12214, doi:10.1029/2009JA01433.

Li, X., D. N. Baker, M. Temerin, T. E. Cayton, G. D. Reeves, R. A. Christensen, J. B. Blake, M. D. Looper, R. Nakamura, and S. G. Kanekal (1997), Multi-Satellite Observations of the Outer Zone Electron Variation During the 3-4 November 1993 Magnetic Storm, J. Geophys. Res., 102, 14123.

Li, W., R. M. Thorne, V. Angelopoulos, J. Bortnik, C. M. Cully, B. Ni, O. LeContel, A. Roux, U. Auster, and W. Magnes (2009), Global distribution of whistler-mode chorus waves observed on the THEMIS spacecraft, Geophys. Res. Lett., 36, L09104, doi:10.1029/2009GL037595.

Li, W., R. M. Thorne, Q. Ma, B. Ni, J. Bortnik, D. N. Baker, H. E. Spence, G. D. Reeves, S. G. Kanekal, J. C. Green, C. A. Kletzing, W. S. Kurth, G. B. Hospodarsky, J. B. Blake, J. F. Fennell and S. G.

Claudepierre (2014a), Radiation belt electron acceleration by chorus waves during the 17 March 2013 storm, J. Geophys. Res. Space Physics, 119, doi:10.1002/2014JA019945.

Li, Z., et al. (2014b), Investigation of EMIC wave scattering as the cause for the BARREL 17 January 2013 relativistic electron precipitation event: A quantitative comparison of simulation with observations, Geophys.Res. Lett., 41, 8722–8729, doi:10.1002/2014GL062273.

Li, W., R. M. Thorne, J. Bortnik, D. N. Baker, G. D. Reeves, S. G. Kanekal, H. E. Spence, and J. C. Green (2015), Solar wind conditions leading to efficient radiation belt electron acceleration: A superposed epoch analysis, Geophys. Res. Lett., 42, 6906–6915, doi:10.1002/2015GL065342.

Li, W., et al. (2013), An unusual enhancement of low-frequency plasmaspheric hiss in the outer plasmasphere associated with substorm-injected electrons, Geophys. Res. Lett., 40, 3798–3803, doi:10.1002/grl.50787.

Liu, W.W., G. Rostoker, and D.N. Baker (1999), Internal acceleration of relativistic electrons by large-amplitude ULF Pc5 pulsations, J. Geophys. Res., 104, 17391-17407.

Liu, W., T. E. Sarris, X. Li, S. R. Elkington, R. Ergun, V. Angelopoulos, J. Bonnell, K. H. Glassmeier (2009), Electric and magnetic field observations of Pc4 and Pc5 pulsations in the inner magnetosphere: A statistical study, J. Geophys. Res., 114, A12206, doi:10.1029/2009JA014243.

Lorentzen, K. R., J. B. Blake, U. S. Inan, and J. Bortnik (2001), Observations of relativistic electron microbursts in association with VLF chorus, J. Geophys. Res., 106, 6017.

Loto'aniu, T.M., H. J. Singer, C. L. Waters, V. Angelopoulos, I. R. Mann, S. R. Elkington, and J. W. Bonnell (2010), Relativistic electron loss due to ultralow frequency waves and enhanced outward radial diffusion, J. Geophys. Res., 115, A12245, doi:10.1029/2010JA015755.

Lyons, L. R., D.-Y. Lee, R. M. Thorne, R. B. Horne, and A. J. Smith (2005), Solar wind-magnetosphere coupling leading to relativistic electron energization during high-speed streams, J. Geophys. Res.,110, A11202, doi:10.1029/2005JA011254.

MacDonald, E.A., M.H.Denton, M.F.Thomsen, and S.P.Gary (2008), Superposed epoch analysis of a whistler instability criterion at geosynchronous orbit during geomagnetic storms, J. Atmos. Solar-Terr. Phys., doi:10.1016/j.jastp.2008.03.021.

Mann, I. R., T. P. O'Brien, and D. K. Milling (2004), Correlations between ULF Pc5 wave power, solar wind speed, and relativistic electron flux in the magnetosphere: solar cycle dependence, Journal of Atmospheric and Solar Terrestrial Physics 66,187-198/j.jastp.2003.10.002.

Mathie, R. A. and I. R. Mann (2000), A correlation between extended intervals of ULF Pc5 wave power and storm-time geosynchronous electron flux enhancements, Geophys. Res. Lett, 27, 3261-3264.

Mathie, R.A. and I.R. Mann (2001), On the solar wind control of Pc5 ULF pulsation power at mid-latitudes: Implications for MeV electron acceleration in the outer radiation belt, J. Geophys. Res., 106, 29,783-29,796, doi:10.1029/2001JA000002.

McPherron, R.L., D.N.Baker, N.U.Crooker (2009), Role of the Russell–McPherron effect in the acceleration of relativistic electrons, J. Atmos. Solar-Terr. Phys., 71(2009)1032–1044.

Meredith, N.P., R.B. Horne, and R. R. Anderson (2001), Substorm dependence of chorus amplitudes: Implications for the acceleration of electrons to relativistic energies, J. Geophys. Res., 106,13,165-13,178, doi: 10.1029/2000JA900156.

Meredith, N. P., R. B. Horne, R. H. A. Iles, R. M. Thorne, D. Heynderickx, and R. R. Anderson (2002), Outer zone relativistic electron acceleration associated with substorm-enhanced whistler mode chorus, J.Geophys. Res., 107(A7), 1144, 10.1029/2001JA900146.

Meredith, N. P., M. Cain, R. B. Horne, R. M. Thorne, D. Summers, R. R. Anderson (2003a), Evidence for chorus-driven electron acceleration to relativistic energies from a survey of geomagnetically disturbed periods, J. Geophys. Res., 108, 1248, doi:10.1029/2002JA009764.

Meredith, N. P., R. B. Horne, R. M. Thorne, and R. R. Anderson (2003b), Favored regions for chorus - driven electron acceleration to relativistic energies in the Earth's outer radiation belt, Geophys. Res. Lett., 30(16), 1871, doi:10.1029/2003GL017698.

Millan, R.M. and R.M. Thorne (2007), Review of radiation belt relativistic electron losses, J. Atmos. Solar-Terr. Phys., 69 (2007) 362–377, doi:10.1016/j.jastp.2006.06.019.

Miyoshi, Y., A. Morioka, T. Obara, H. Misawa, T. Nagai, and Y. Kasahara (2003), Rebuilding process of the outer radiation belt during the 3 November 1993 magnetic storm: NOAA and Exos-D observations, J. Geophys. Res., 108, NO. A1, 1004, doi:10.1029/2001JA007542.

Miyoshi, Y., A. Morioka, R. Kataoka, Y. Kasahara, and T. Mukai (2007), Evolution of the outer radiation belt during the November 1993 storms driven by corotating interaction regions, J. Geophys. Res., 112, A05210, doi:10.1029/2006JA012148.

Miyoshi, Y., K. Sakaguchi, K. Shiokawa, D. Evans, J. Albert, M. Connors, and V. Jordanova (2008), Precipitation of radiation belt electrons by EMIC waves, observed from ground and space, Geophys. Res. Lett., 35, L23101, doi:10.1029/2008GL035727.

Miyoshi, Y., R. Kataoka, Y. Kasahara, A. Kumamoto, T. Nagai, and M. F. Thomsen (2013), High-speed solar wind with southward interplanetary magnetic field causes relativistic electron flux enhancement of the outer radiation belt via enhanced condition of whistler waves, Geophys. Res. Lett., 40, doi:10.1002/grl.50916.

Morley, S. K., R. H. W. Friedel, T. E. Cayton, and E. Noveroske (2010), A rapid, global and prolonged electron radiation belt dropout observed with the Global Positioning System constellation, Geophys. Res. Lett., 37, L06102, doi:10.1029/2010GL042772.

Mourenas, D., A. V. Artemyev, O. V. Agapitov, F. S. Mozer, and V. V. Krasnoselskikh (2016), Equatorial electron loss by double resonance with oblique and parallel intense chorus waves, J. Geophys. Res. Space Physics, 121, 4498–4517,doi:10.1002/2015JA022223.

Nakamura, R., J.B Blake, S.R Elkington, D.N Baker, W Baumjohann, B Klecker (2002) Relationship between ULF Pc5 waves and radiation belt electrons during the March 10, 1998, storm, Advances in Space Research, Volume 30, Issue 10, November 2002, Pages 2163-2168.

Neter, J., W. Wasserman, and M. H. Kutner (1985), Applied Linear Statistical Models, Richard D. Irwin, Inc., Homewood, Ill.

Newell, P. T., T. Sotirelis, K. Liou, C.-I. Meng, and F. J. Rich (2006), Cusp latitude and the optimal solar wind coupling function, J. Geophys. Res., 111, A09207, doi:10.1029/2006JA011731.

Newell, P. T., and J. W. Gjerloev (2011), Evaluation of SuperMAG auroral electrojet indices as indicators of substorms and auroral power, J. Geophys. Res., 116, A12211, doi:10.1029/2011JA016779.

Ni, B., Z. Xiang, X. Gu, Y. Y. Shprits, C. Zhou, Z. Zhao, X. Zhang, and P. Zuo (2016), Dynamic responses of the Earth's radiation belts during periods of solar wind dynamic pressure pulse based on normalized superposed epoch analysis, J. Geophys. Res. Space Physics, 121, 8523–8536, doi:10.1002/2016JA023067.

O’Brien, T. P., and R. L. McPherron, (2003) An empirical dynamic equation for energetic electrons at geosynchronous orbit, J. Geophys. Res., 108(A3), 1137, doi:10.1029/2002JA009324.

O'Brien, T. P., K. R. Lorentzen, I. R. Mann, N. P. Meredith, J. B. Blake, J. F. Fennell, M. D. Looper, D. K. Milling, and R. R. Anderson (2003), Energization of relativistic electrons in the presence of ULF Pc5 power and MeV microbursts: Evidence for dual ULF Pc5 and VLF acceleration, J. Geophys. Res., 108, 1329, doi:10.1029/2002JA009784.

O’Brien, T. P., M. D. Looper, and J. B. Blake (2004), Quantification of relativistic electron microburst losses during the GEM storms, Geophys. Res. Lett., 31, L04802, doi:10.1029/2003GL018621.

Onsager, T. G., G. Rostoker, H.-J. Kim, G. D. Reeves, T. Obara, H. J. Singer, and C. Smithtro, (2002), Radiation belt electron flux dropouts: Local time, radial, and particle-energy dependence, J. Geophys. Res., 107(A11), 1382, doi:10.1029/2001JA000187.

Orlova, K. G. and Y.Y. Shprits (2010), Dependence of pitch - angle scattering rates and loss timescales on the magnetic field model, Geophys. Res. Lett., 37, L05105, doi:10.1029/2009GL041639.

Ozeke, L. G., I. R. Mann, K. R. Murphy, D. G. Sibeck, and D. N. Baker (2017), Ultra-relativistic radiation belt extinction and ULF Pc5 wave radial diffusion: Modeling the September 2014 extended dropout event, Geophys. Res. Lett., 44, doi:10.1002/2017GL072811.

Paulikas, G. A., and J. B. Blake (1979), Effects of the solar wind on magnetospheric dynamics: Energetic electrons at the synchronous orbit. In: Olson W P (Ed) Quantitative Modelling of Magnetospheric Processes, American Geophysical Union Geophysical Monograph 21,180-202.

Pilipenko, V., Yagova, N., Romanova, N., and J. Allen, (2006), Statistical relationships between satellite anomalies at geostationary orbit and high-energy particles. Adv. Space Res. 37, 1192–1205.

Rae, I. J., et al. (2005), Evolution and characteristics of global Pc5 ULF waves during a high solar wind speed interval, J. Geophys. Res., 110, A12211, doi:10.1029/2005JA011007.

Reeves, G. D., K. L. McAdams, R. H. W. Friedel, and T. P. O'Brien, Acceleration and loss of relativistic electrons during geomagnetic storms, Geophys. Res. Lett., 30(10), 1529, doi:10.1029/2002GL016513, 2003.

Reeves, G. D., S. K. Morley, R. H. W. Friedel, M. G. Henderson, T. E. Cayton, G. Cunningham, J. B. Blake, R. A. Christensen, and D. Thomsen (2011), On the relationship between relativistic electron flux and solar wind velocity: Paulikas and Blake revisited, J. Geophys. Res., 116, A02213, doi:10.1029/2010JA015735.

Reeves, G. D., et al. (2013), Electron acceleration in the heart of the Van Allen radiation belts, Science, 341, 999–994, doi:10.1126/science.1237743.

Regi, M., M. de Lauretis, and P. Francia (2015), Pc5 geomagnetic fluctuations in response to solar wind excitation and their relationship with relativistic electron fluxes in the outer radiation belt ,Earth, Planets and Space 67:9 DOI 10.1186/s40623-015-0180-8.

Ren, J., Q. G. Zong, Y. F. Wang, and X. Z. Zhou (2015), The interaction between ULF Pc5 waves and thermal plasma ions at the plasmaspheric boundary layer during substorm activity, J. Geophys. Res. Space Physics, 120, 1133–1143, doi:10.1002/2014JA020766.

Rodger, C. J., T. Raita, M. A. Clilverd, A. Seppälä, S. Dietrich, N. R. Thomson, and T. Ulich (2008), Observations of relativistic electron precipitation from the radiation belts driven by EMIC waves, Geophys. Res. Lett., 35, L16106, doi:10.1029/2008GL034804.

Rodger, C. J., A. T. Hendry, M. A. Clilverd, C. A. Kletzing, J. B. Brundell, and G. D. Reeves (2015), High-resolution in situ observations of electron precipitation-causing EMIC waves, Geophys. Res. Lett., 42, 9633–9641, doi:10.1002/2015GL066581.

Rodger, C.J., K.Cresswell-Moorcock, and M.A.Clilverd (2016), Nature's Grand Experiment: Linkage between magnetospheric convection and the radiation belts, J. Geophys. Res. Space Physics, 121,171–189, doi:10.1002/2015JA02153.

Romanova, N., V. Pilipenko, N. Crosby, and O. Khabarova (2007), ULF Pc5 Wave Index and Its Possible Applications in Space Physics, Bulg. J. Phys. 34 (2007) 136–148.

Rostoker, G., S. Skone, and D.N. Baker (1998), On the origin of relativistic electrons in the magnetosphere associated with some geomagnetic storms, Geophys. Res. Lett., 25, doi: 10.1029/98GL02801.

Saikin, A. A., J.-C. Zhang, C. W. Smith, H. E. Spence, R. B. Torbert, and C. A. Kletzing (2016), The dependence on geomagnetic conditions and solar wind dynamic pressure of the spatial distributions of EMIC waves observed by the Van Allen Probes, J. Geophys. Res. Space Physics, 121, 4362–4377, doi:10.1002/2016JA022523.

Sakaguchi, K., Y. Miyoshi, S. Saito, T. Nagatsuma, K. Seki and K. T. Murata (2015), Relativistic electron flux forecast at geostationary orbit using Kalman filter based on multivariate autoregressive models, Space Weather, 11, doi:10.1002/swe.20020.

Shah, A., C. L. Waters, M. D. Sciffer, F. W. Menk, and R. L. Lysak (2015), Effect of the ionosphere on the interaction between ULF Pc5 waves and radiation belt electrons, J. Geophys. Res. Space Physics, 120, 8572–8585,

Shah, A., C. L. Waters, M. D. Sciffer, and F. W. Menk (2016), Energization of outer radiation belt electrons during storm recovery phase, J. Geophys. Res. Space Physics, 121, 10,845–10,860, doi:10.1002/2016JA023245.

Shprits, Y.Y., R.M. Thorne, R. Friedel, G.D. Reeves, J. Fennell, D.N. Baker, and S.G. Kanekal (2006), Outward radial diffusion driven by losses at magnetopause, J. Geophys. Res., 111, A11214, doi:10.1029/2006JA011657.

Sibeck, D.G., R.E. Lopez, and E.C. Roelof (1991), Solar wind control of the magnetopause shape, location, and motion, J. Geophys. Res., 96, NO. A4, PAGES 5489-5495, doi: 10.1029/90JA02464.

Simms, L. E., V. A. Pilipenko, and M. J. Engebretson (2010), Determining the key drivers of magnetospheric Pc5 wave power, J. Geophys. Res., 115, A10241, doi:10.1029/2009JA015025.

Simms, L. E., M. J. Engebretson, A.J. Smith, M. Clilverd, V.A. Pilipenko, and G.D. Reeves (2014), Prediction of relativistic electron flux following storms at geostationary orbit: multiple regression analysis, J. Geophys. Res. Space Physics, 119, 10.1002/2014JA019955.

Simms, L. E., V.A. Pilipenko, M. J. Engebretson, G.D. Reeves, A.J. Smith, M. Clilverd, (2015), Analysis of the effectiveness of ground-based VLF wave observations for predicting or nowcasting relativistic electron flux at geostationary orbit*,* J. Geophys. Res. Space Physics*,* 120*,* doi:10.1002/2014JA020337.

Simms, L. E., M. J. Engebretson, V. Pilipenko, G. D. Reeves, and M. Clilverd (2016), Empirical predictive models of daily relativistic electron flux at geostationary orbit: Multiple regression analysis, J. Geophys. Res. Space Physics, 121, 3181–3197, doi:10.1002/2016JA022414.

Simms, L.E., M. J. Engebretson, M. A. Clilverd, C. J. Rodger, M. R. Lessard, and G. D. Reeves (2018b – Paper 2), Nonlinear and synergistic effects of ULF Pc5, VLF chorus, and EMIC waves on relativistic electron flux at geosynchronous orbit, submitted.

Smith, A.J., N. P. Meredith, and T.P. O'Brien (2004), Differences in ground-observed chorus in geomagnetic storms with and without enhanced relativistic electron fluxes, J. Geophys. Res., 109, A11204, doi:10.1029/2004JA010491.

Smith, A. J., R. B. Horne, and N. P. Meredith (2010), The statistics of natural ELF/VLF waves derived from a long continuous set of ground-based observations at high latitude, J. Atmos. Terr. Phys., 72, 463–475.

Spasojevic, M. and U.S. Inan (2005), Ground based VLF observations near L = 2.5 during the Halloween 2003 storm, Geophys. Res. Lett., 32, L21103, doi:10.1029/2005GL024377.

Su, Z., et al. (2014), Intense duskside lower band chorus waves observed by Van Allen Probes: Generation and potential acceleration effect on radiation belt electrons, J. Geophys. Res. Space Physics, 119, 4266–4273, doi:10.1002/2014JA019919.

Su Z., H. Zhu, F. Xiao, Q.-G. Zong, X.-Z. Zhou, H. Zheng, Y. Wang, S. Wang, Y.-X. Hao, Z. Gao, Z. He, D.N. Baker, H.E. Spence, G.D. Reeves, J.B. Blake, and J.R. Wygant (2015), Ultra-low-frequency wave-driven diffusion of radiation belt relativistic electrons, Nat. Comm., doi: 10.1038/ncomms10096.

Summers, D., R. M. Thorne, and F. Xiao (1998), Relativistic theory of wave-particle resonant diffusion with application to electron acceleration in the magnetosphere, J. Geophys. Res., 103, 20,487.

Summers, D. and C. Ma (2000), Rapid acceleration of electrons in the magnetosphere by fast-mode MHD waves, J. Geophys. Res., 105, 15,887-15895.

Summers, D., B. Ni, and N. P. Meredith (2007), Timescales for radiation belt electron acceleration and loss due to resonant wave-particle interactions: 2. Evaluation for VLF chorus, ELF hiss, and electromagnetic ion cyclotron waves, J. Geophys. Res., 112, A04207, doi:10.1029/2006JA011993.

Summers, D. and R.M. Thorne (2003), Relativistic electron pitch-angle scattering by electromagnetic ion cyclotron waves during geomagnetic storms, J. Geophys. Res., 108, NO. A4, 1143, doi:10.1029/2002JA009489.

Takahashi, K. and A. Y. Ukhorskiy (2007), Solar wind control of Pc5 pulsation power at geosynchronous orbit, J. Geophys. Res., 112, A11205, doi:10.1029/2007JA012483.

Tan, L. C., X. Shao, A. S. Sharma, and S. F. Fung (2011), Relativistic electron acceleration by compressional-mode ULF Pc5 waves: Evidence from correlated Cluster, Los Alamos National Laboratory spacecraft, and ground-based magnetometer measurements, J. Geophys. Res., 116, A07226, doi:10.1029/2010JA016226.

Tang, C. L., J.-C. Zhang, G. D. Reeves, Z. P. Su, D. N. Baker, H. E. Spence, H. O. Funsten, J. B. Blake, and J. R. Wygant (2016), Prompt enhancement of the Earth's outer radiation belt due to substorm electron injections, J. Geophys. Res. Space Physics, 121, 11,826–11,838, doi:10.1002/2016JA023550.

Tang, C. L., Y. X. Wang, B. Ni, J.-C. Zhang, G. D. Reeves, Z. P. Su, D. N. Baker,H. E. Spence, H. O. Funsten, and J. B. Blake (2017), Radiation belt seed population and its association with the relativistic electron dynamics: A statistical study, J. Geophys. Res. Space Physics, 122, doi:10.1002/2017JA023905.

Tetrick, S. S., et al. (2017), Location of intense electromagnetic ion cyclotron (EMIC) wave events relative to the plasmapause: Van Allen Probes observations, J. Geophys. Res. Space Physics, 122, 4064-4088, doi:10.1002/2016JA023392.

Thorne, R.M. (2010), Radiation belt dynamics: The importance of wave ‐ particle interactions, Geophys. Res. Lett., 37, L22107, doi:10.1029/2010GL044990.

Thorne, R. M., W. Li, B. Ni, Q. Ma, J. Bortnik, L. Chen, D. N. Baker, H. E. Spence, G. D. Reeves, M. G. Henderson, C. A. Kletzing, W. S. Kurth, G. B. Hospodarsky, J. B. Blake, J. F. Fennell, S. G. Claudepierre, and S. G. Kanekal (2013), Rapid local acceleration of relativistic radiation-belt electrons by magnetospheric chorus, Nature, 504, 411, doi:10.1038/nature12889.

Tsurutani, B. T., and E. J. Smith (1974), Postmidnight chorus: A substorm phenomenon, J. Geophys. Res., 79, 118–127, doi:10.1029/JA079i001p00118.

Tsurutani, B. T. and Edward J. Smith (1977), Two types of magnetospheric ELF chorus and their substorm dependences, J. Geophys. Res., 82, 5112-5128, doi: 10.1029/JA082i032p05112.

Turner, D.L., V. Angelopoulos, W. Li, M. D. Hartinger, M. Usanova, I. R. Mann, J. Bortnik, and Y. Shprits (2013), On the storm-time evolution of relativistic electron phase space density in Earth's outer radiation belt, J. Geophys. Res.: Space Physics, 118, 2196–2212, doi:10.1002/jgra.50151.

Turner, D. L., V. Angelopoulos, W. Li, J. Bortnik, B. Ni, Q.Ma, R. M. Thorne, S. K. Morley, M. G. Henderson, G. D. Reeves, M. Usanova, I. R. Mann, S. G. Claudepierre, J. B. Blake, D. N. Baker, C.-L. Huang, H. Spence, W. Kurth, C. Kletzing, and J. V. Rodriguez (2014), Competing source and loss mechanisms due to wave-particle interactions in Earth's outer radiation belt during the 30 September to 3 October 2012 geomagnetic storm, J. Geophys. Res. Space Physics, 119, 1960–1979, doi:10.1002/2014JA019770.

Turner, D. L., et al. (2015), Energetic electron injections deep into the inner magnetosphere associated with substorm activity, Geophys. Res. Lett., 42, 2079–2087, doi:10.1002/2015GL063225.

Ukhorskiy, A. Y., M. I. Sitnov, A. S. Sharma, B. J. Anderson, S. Ohtani, and A. T. Y. Lui (2004), Data-derived forecasting model for relativistic electron intensity at geosynchronous orbit, Geophys. Res. Lett., 31, L09806, doi:10.1029/2004GL019616.

Ukhorskiy, A.Y., K. Takahashi, B.J. Anderson, and H. Korth (2005), Impact of toroidal ULF Pc5 waves on the outer radiation belt electrons, J. Geophys. Res., 110, A10202, doi:10.1029/2005JA011017.Ukhorskiy, A. Y., B. J. Anderson, K. Takahashi, and N. A. Tsyganenko (2006), Impact of ULF Pc5 oscillations in solar wind dynamic pressure on the outer radiation belt electrons, Geophys. Res. Lett., 33, L06111, doi:10.1029/2005GL024380.

Ukhorskiy, A.Y., M.I. Sitnov, K. Takahashi, and B.J. Anderson (2009), Radial transport of radiation belt electrons due to stormtime Pc5 waves, Ann. Geophys., 27, 2173–2181.

Ukhorskiy, A. Y., Y. Y. Shprits, B. J. Anderson, K. Takahashi, and R. M. Thorne (2010), Rapid scattering of radiation belt electrons by storm-time EMIC waves, Geophys. Res. Lett., 37, L09101, doi:10.1029/2010GL042906.

Ukhorskiy, A. Y., M. I. Sitnov, R. M. Millan, B. T. Kress, J. F. Fennell, S. G. Claudepierre, and R. J. Barnes (2015), Global storm time depletion of the outer electron belt, J. Geophys. Res. Space Physics, 120, 2543–2556, doi:10.1002/2014JA020645.

Usanova, M. E., I. R. Mann, J. Bortnik, L. Shao, and V. Angelopoulos (2012), THEMIS observations of electromagnetic ion cyclotron wave occurrence: Dependence on AE, SYMH, and solar wind dynamic pressure, J. Geophys. Res., 117, A10218, doi:10.1029/2012JA018049.

Usanova, M. E., A. Drozdov, K. Orlova, I. R. Mann, Y. Shprits, M. T. Robertson, D. L. Turner, D. K. Milling, A. Kale, D. N. Baker, S. A. Thaller, G. D. Reeves, H. E. Spence, C. Kletzing, and J. Wygant (2014), Effect of EMIC waves on relativistic and ultrarelativistic electron populations: Ground-based and Van Allen Probes observations, Geophys. Res. Lett., 41, 1375–1381, doi:10.1002/2013GL059024.

Walker, A. D. M. (1981), The Kelvin-Helmholtz instability in the low-latitude boundary layer. Planet. Space Sci. 29, 1119–1133 http://dx.doi.org/10.1016/0032-0633(81)90011-8.

Xiao, F., C. Yang, Z. Su, Q. Zhou, Z. He, Y. He, D.N. Baker, H.E. Spence, H.O. Funsten, and J.B. Blake (2015), Wave-driven butterfly distribution of Van Allen belt relativistic electrons, Nature Comm., DOI: 10.1038/ncomms9590.

Yu, Y., J. Koller, and S. K. Morley (2013), Quantifying the effect of magnetopause shadowing on electron radiation belt dropouts, Ann. Geophys., 31, 1929–1939, doi:10.5194/angeo-31-1929-2013.

Yuan, C., and Q. Zong (2013), Relativistic electron fluxes dropout in the outer radiation belt under different solar wind conditions, J. Geophys. Res. Space Physics, 118, 7545–7556, doi:10.1002/2013JA019066.

Zhao, H., D. N. Baker, A. N. Jaynes, X. Li, S. R. Elkington, S. G. Kanekal, H. E. Spence, A. J. Boyd, C.-L. Huang, and C. Forsyth (2017), On the relation between radiation belt electrons and solar wind parameters/geomagnetic indices: Dependence on the first adiabatic invariant and L*, J. Geophys. Res. Space Physics, 122, 1624–1642, doi:10.1002/2016JA023658.

Zong, Q.G., Y. F. Wang, H. Zhang, S. Y. Fu, H. Zhang, C. R. Wang, C. J. Yuan, and I. Vogiatzis (2012), Fast acceleration of inner magnetospheric hydrogen and oxygen ions by shock induced ULF Pc5 waves, J. Geophys. Res., 117, A11206, doi:10.1029/2012JA018024.

Table 1. Unstandardized regression coefficients from multiple regressions for each of four energy channels for models of Figure 5 (see figure for standardized coefficients). These unstandardized coefficients could be used in a modified version of Equation 2 to predict relativistic electron.

*: significant effect at $p < 0.05$.

	0.7-1.8MeV	1.8-3.5MeV	3.5-6.0MeV	6.0-7.8MeV
Constant	-.2728254	-.4030948*	.4691164*	-.0611605
Pressure	-.0228033*	-.0310316*	-.0613575*	-.0255279*
|B|	-.0321384*	-.0357031*	-.0176730*	-.0079075*
Dst	-.0013783	-.0011421	.0021548*	.0000890
Bz	-.0000013	.0002284	-.0002250	.0006029*
N	.0011050	-.0114411*	-.0102755*	-.0008994
V	.0001995	.0003322	.0002628	.0003143*
Substorms	-.0017459	.0051601	.0181378*	.0096554*
Source electrons	.0043594	-.0289915	-.0542447	-.0574846*
ULF Pc5	.0047903*	.0062157*	.0035429*	-.0002297
Chorus	.0807329*	.1138711*	.0939481*	.0293270*
EMIC	-.0056024	-.0069559	-.0162118*	-.0049493*
Seed electrons	.1919567*	.1572711*	-.0731433*	-.0217932
Log high energy electron flux (AR)	.7221844*	.7359866*	.8907230*	.7935746*
R^2	.884	.892	.905	.817
Correlation	.940	.944	.951	.904

Figure 1. Summary of the drivers of enhancement and loss processes of relativistic energy electrons. Temporary effects are in gray text.

Figure 2. Distributed lag regression models for individual predictors. Lags 0-5 in combination are used to predict relativistic electron flux. Each bar gives the regression coefficient for that particular lag. Bars with black outlines are autoregressive models where lag 1 flux is added as a predictor. Bars outlined in gray do not include the autoregressive term.

Figure 3. Standardized regression coefficients of the combined analyses of internal effects: ULF Pc5, chorus, and EMIC waves, seed electron flux (270 keV), and Dst at lags 0-2; pressure and |B| at lag 0. Statistically significant terms are shown in dark gray. The autoregressive component (lag 1 of relativistic electron flux) was also included in these models, but is not shown in the figures. Its standardized regression coefficient varied from .792-.921. R^2 are 0.899, 0.901, 0.916, and 0.810 for the four energy channels (0.7-1.8, 1.8-3.5, 3.5-6.0, and 6.0-7.8, respectively). The square root of these (corresponding to a correlation coefficient) are 0.948, 0.950, 0.957, and 0.900.

Figure 4. Standardized regression coefficients of the combined analyses of external effects: % hours/day of Bz<0, V, pressure, and |B| with intermediaries substorms and source electron flux. Statistically significant terms ($p < 0.05$) are shown in dark gray. The autoregressive component (lag 1 of relativistic electron flux) was also included in these models, but is not shown in the figures. Its standardized regression coefficient varied from .750-.907. R^2 are 0.886, 0.895, 0.903, and 0.808 for the four energy channels (0.7-1.8, 1.8-3.5, 3.5-6.0, and 6.0-7.8, respectively). The square root of these (corresponding to a correlation coefficient) are 0.941, 0.946, 0.950, and 0.899.

Figure 5. Standardized regression coefficients from multiple regression for each of four energy channels with all predictors: lag 0 Pressure, |B|, and Dst; lag 1 Bz, V, substorms, source electron flux, ULF Pc5, chorus, and EMIC wave activity; seed electron flux. Lag 1 log relativistic electron flux is included as an autoregressive term (not shown in figure). Dark gray bars show significant effects ($p < 0.05$). Regression coefficients for the autoregressive term ranged from 0.724- 0.892. Unstandardized regression coefficients and fraction of variation explained by the model (the R^2 or prediction efficiency) are given in Table 1 for this model, along with the square root of the R^2 which is equivalent to a correlation coefficient.

Figure 1.

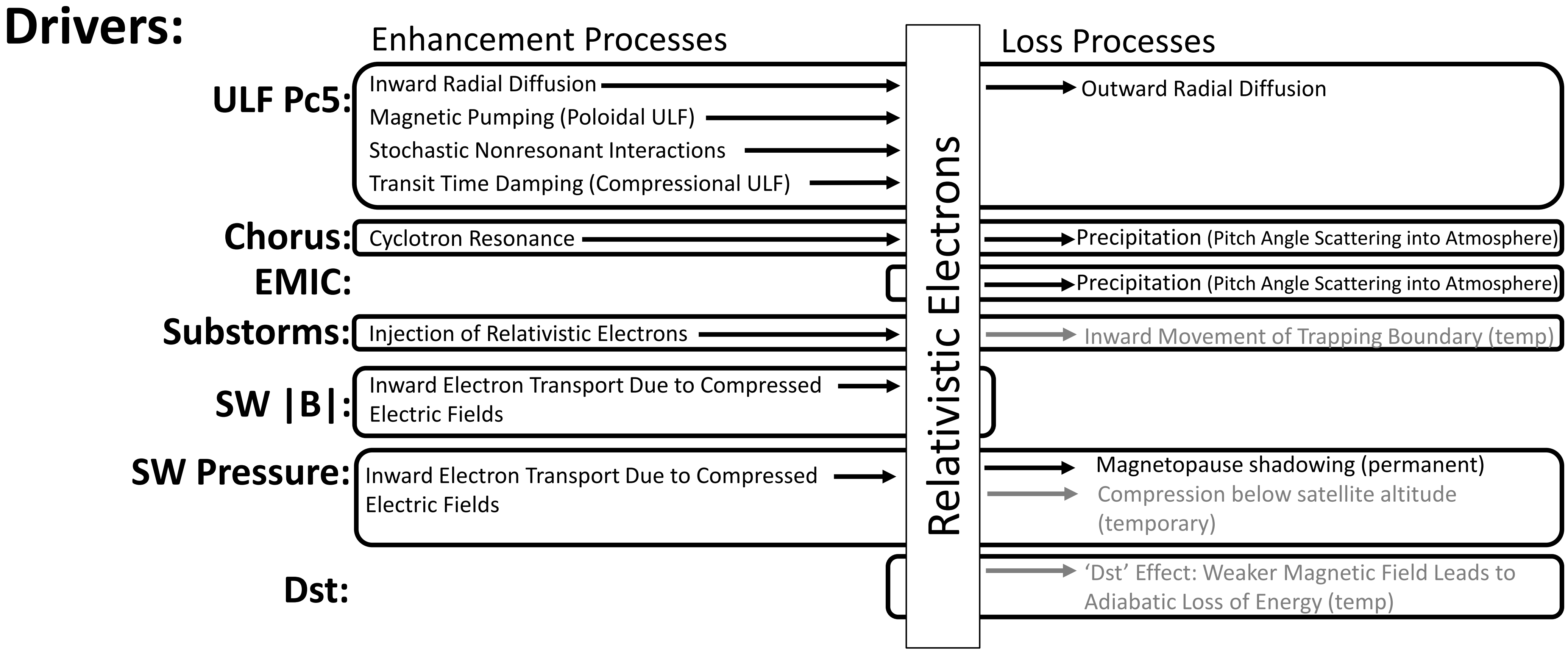
Drivers:
Enhancement Processes
Loss Processes
Relativistic Electrons
ULF Pc5:
Inward Radial Diffusion
Magnetic Pumping (Poloidal ULF)
Stochastic Nonresonant Interactions
Transit Time Damping (Compressional ULF)
Outward Radial Diffusion
Chorus:
Cyclotron Resonance
Precipitation (Pitch Angle Scattering into Atmosphere)
EMIC:
Precipitation (Pitch Angle Scattering into Atmosphere)
Substorms:
Injection of Relativistic Electrons
Inward Movement of Trapping Boundary (temp)
SW |B|:
Inward Electron Transport Due to Compressed Electric Fields
SW Pressure:
Inward Electron Transport Due to Compressed Electric Fields
Magnetopause shadowing (permanent)
Compression below satellite altitude (temporary)
Dst:
'Dst' Effect: Weaker Magnetic Field Leads to Adiabatic Loss of Energy (temp)

Figure 2.

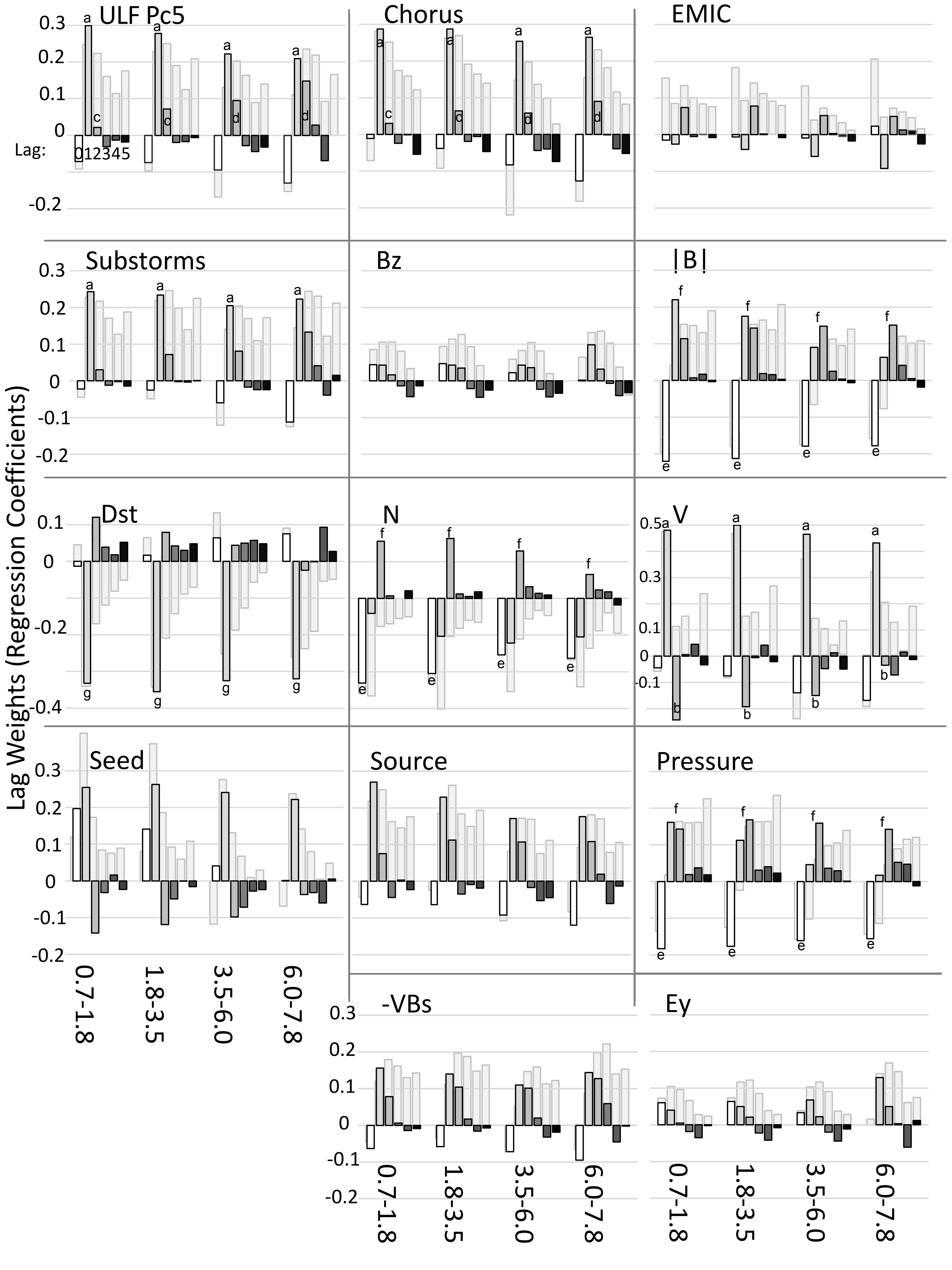

Lag Weights (Regression Coefficients)
ULF Pc5
Chorus
EMIC
Substorms
Bz
|B|
Dst
N
V
Seed
Source
Pressure
-VBs
Ey
Lag:
012345
0.7-1.8
1.8-3.5
3.5-6.0
6.0-7.8

Figure 3.

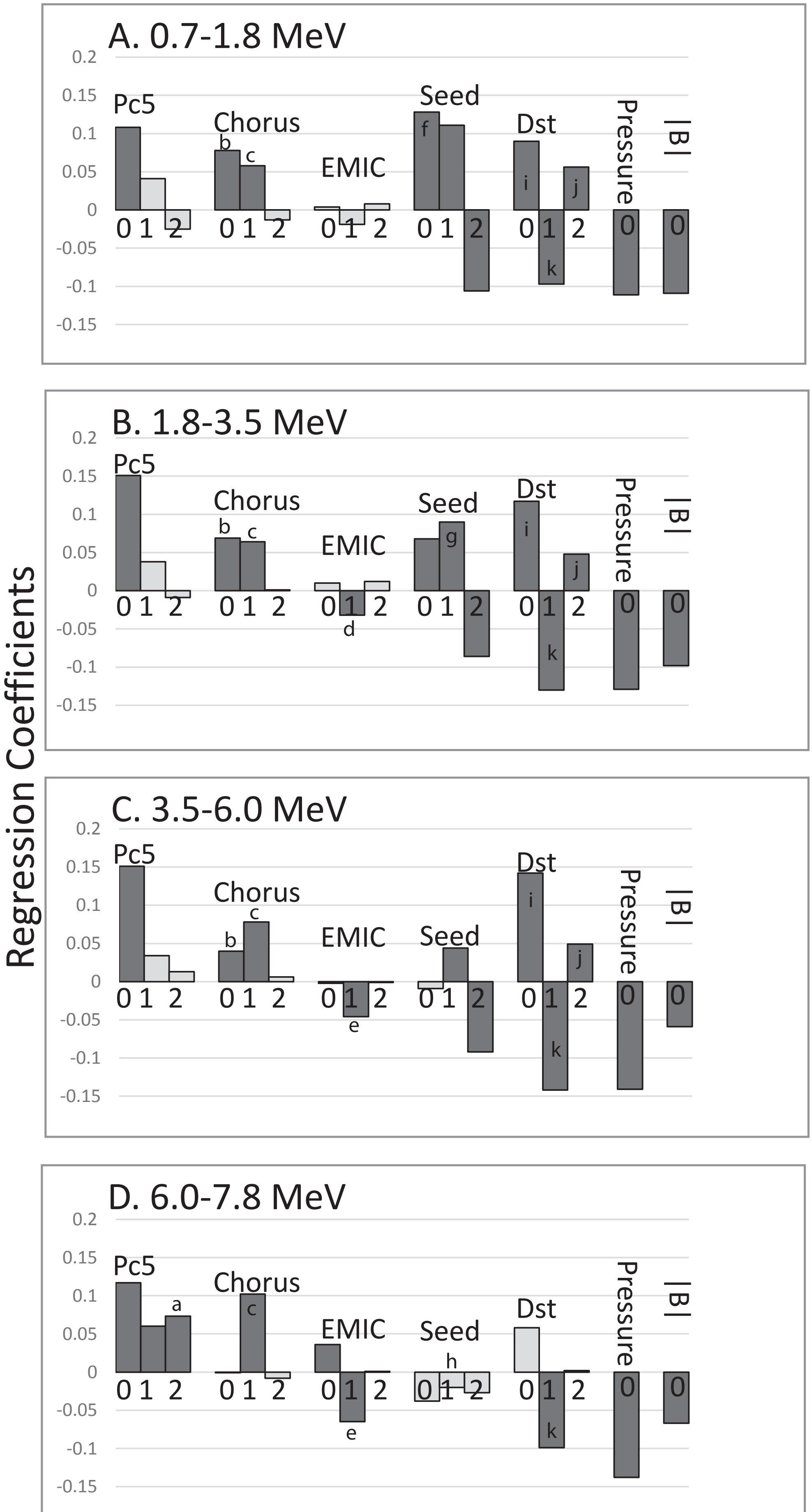

Regression Coefficients
A. 0.7-1.8 MeV
B. 1.8-3.5 MeV
C. 3.5-6.0 MeV
D. 6.0-7.8 MeV
0.2
0.15
0.1
0.05
0
-0.05
-0.1
-0.15
Pc5
Chorus
EMIC
Seed
Dst
Pressure
|B|
0 1 2
a
b
c
d
e
f
g
h
i
j
k

Figure 4.

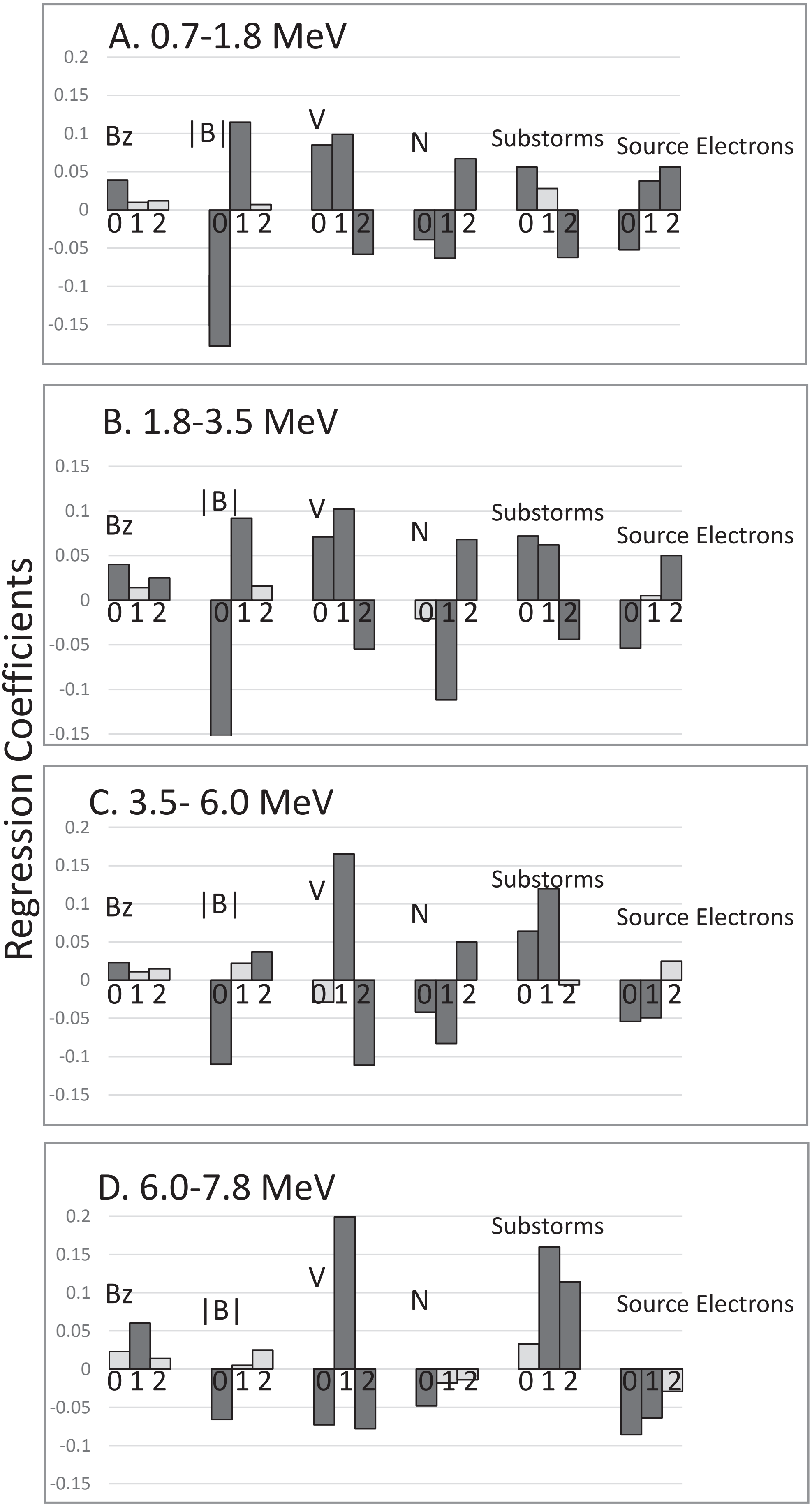
Regression Coefficients
A. 0.7-1.8 MeV
B. 1.8-3.5 MeV
C. 3.5- 6.0 MeV
D. 6.0-7.8 MeV
Bz
|B|
V
N
Substorms
Source Electrons
0 1 2
0.2
0.15
0.1
0.05
0
-0.05
-0.1
-0.15

Figure 5.

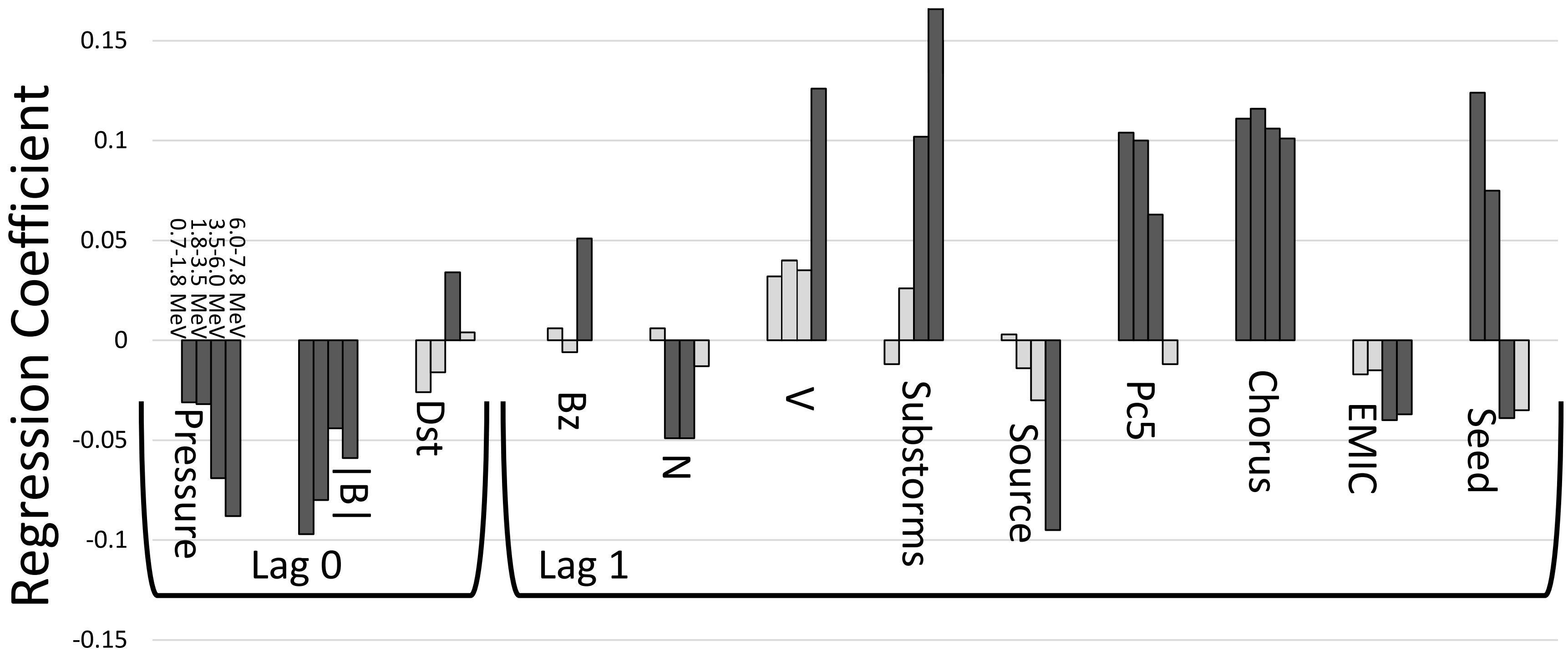

Regression Coefficient
0.15
0.1
0.05
0
-0.05
-0.1
-0.15
0.7-1.8 MeV
1.8-3.5 MeV
3.5-6.0 MeV
6.0-7.8 MeV
Pressure
|B|
Dst
Lag 0
Bz
N
V
Substorms
Source
Pc5
Chorus
EMIC
Seed
Lag 1